Acta Materialia 107 (2016) 102–126

Contents lists available at ScienceDirect

Acta Materialia

journal homepage: www.elsevier.com/locate/actamat

Full length article

On the crystallization of graphite from liquid iron–carbon–silicon melts

D.M. Stefanescu [a, b, *], G. Alonso [c], P. Larrañaga [c], E. De la Fuente [c], R. Suarez [d]

[a] The Ohio State University, Columbus, OH, USA
[b] The University of Alabama, Tuscaloosa, AL, USA
[c] Área Ingeniería, I+D y Procesos Metalúrgicos, IK4-Azterlan, Durango, Bizkaia, Spain
[d] Veigalan Estudio 2010, Durango, Bizkaia, Spain

ARTICLE INFO

Article history:
Received 15 December 2015
Received in revised form
20 January 2016
Accepted 21 January 2016
Available online xxx

Keywords:
Cast iron
Graphite morphology
Foliated dendrites
Compacted graphite
Spheroidal graphite
Solidification

ABSTRACT

Extensive SEM work was carried out on deep etched specimens to reveal the evolution of graphite shape in Fe–C–Si alloys of industrial composition during early solidification and at room temperature. The samples had various magnesium and titanium levels designed to produce graphite morphologies ranging from coarse lamellar to interdendritic lamellar to mixed compacted – spheroidal. The present findings were then integrated in previous knowledge to produce an understanding of the crystallization of lamellar, compacted and spheroidal graphite.

It was demonstrated that most forms of graphite grow radially from a common center, most of the time as foliated dendrites (see Figure). The basic building blocks of the graphite aggregates are hexagonal faceted graphite platelets with nanometer height and micrometer width. During solidification, thickening of the platelets occurs through growth of additional graphene layers nucleated at the ledges of the graphite prism. In the magnesium-free irons that graphite platelets assemble into foliated crystals and dendrites, forming graphite plates that grow along the *a*-axis. In the magnesium-modified melts the graphite platelets stack along the *c*-axis, producing clusters with random orientation. The clusters are then assembled into quasi-cylindrical shapes connected to more or less curved walls to form tadpole graphite, compacted graphite, or chunky graphite. If enough magnesium is added, conical sectors made of platelets stacked in the *c*-direction grow from the same nucleus. The conical sectors may occupy the whole volume of the sphere forming a graphite spheroid, or only part of it like in chunky graphite. The large number of cavities observed between the platelets is consistent with growth of foliated dendrites.

1. Background

Multicomponent Fe–C–Si–Mn–S-etc. alloys, known in industry as cast irons, solidify with a stable austenite/graphite (γ/Gr), or metastable γ/Fe_3C eutectic. Although the use of these alloys in the panoply of materials employed by humans dates as far back as 502 B.C., and in spite of the extensive research started at the beginning of the 18th century and continued to these days, unanswered questions regarding the mechanism of formation of various graphite shapes are still waiting for answers.

1.1. Graphite morphologies and crystal lattice

Depending on composition and cooling rate, three main graphite morphologies crystallize from the Fe–C–Si melt during solidification: lamellar (LG), compacted or vermicular (CG) and spheroidal (SG), as exemplified in Fig. 1 [1–3]. The internal structure of SG exhibits conical sectors of parallel graphite planes growing radially from the center (Fig. 2-a). The sectors may be partially broken (Fig. 2-b) in extreme cases causing “exploded” graphite. The annular rings may exhibit zig-zag steps of the (0001) planes, suggesting columnar crystals of graphite with different orientations [4].

The compacted graphite is considered to be an intermediate shape between LG and SG. The highly 3D branched morphology of CG was revealed as early as 1979 through successive polishing and reconstruction of the two-dimensional (2-D) microstructure [5]

* Corresponding author. The Ohio State University, Columbus, OH, USA.
E-mail address: stefanescu.1@osu.edu (D.M. Stefanescu).

http://dx.doi.org/10.1016/j.actamat.2016.01.047
1359-6454/

(Fig. 3-a), and then confirmed through deep etching (Fig. 1-b), and graphite extraction through focused ion beam nano-tomography [6] (Fig. 3-b).

The LG is further classified as a function of size and distribution. The most common shapes of lamellar graphite are coarse lamellar (type-A) and interdendritic (type-D, and type-E often referred to as undercooled graphite). Very fine interdendritic graphite can be obtained for example in irons with normal sulfur content of 0.03–0.08wt%, high titanium (0.5–1%) and high cooling rates [7].

Other intermediate graphite shapes have been identified, such as coral graphite, a highly branched fibrous type of graphite [8,9], and superfine interdendritic graphite (SIG), which is short (10–20 μm) and stubby, exhibiting round edges similar to the coral graphite. It was obtained in low-S and moderate-Ti content irons (*e.g.* <0.01%S, ~0.3%Ti) [10].

Several irregular and undesired graphite shapes are considered to be the outcome of degeneration of SG. Chunky graphite (Fig. 4) appears as a result of extensive branching of graphite spheroids [11,12]. It is a highly interconnected form of graphite that does not include broken pieces of graphite spheroids.

A transition LG-to-CG-to-SG can be triggered through the addition of small amounts of Mg, Ce or lanthanides to a low sulfur iron. The process is reversible: SG will revert to LG with sulfur addition or through loss of magnesium by evaporation and/or oxidation.

Alternatively, similar structural changes can be achieved by holding molten iron in vacuum for long periods (days or weeks) prior to casting to remove elements such as oxygen, sulfur and phosphorus, leaving a "clean" melt [13,14]. Dhindaw and Verhoeven [15] observed SG in vacuum-melted high purity Fe–C–Si alloys of hypoeutectic and eutectic compositions solidified at high cooling rates. These observations lead some researchers to suggest that the spheroidal form is actually the preferred habit for growth from a metallic solution, in the absence of surface active elements such as O, S and P, and that LG is an impurity-modified form [16].

While in industrial practice the transition between these graphite shapes is controlled reasonably well, in spite of the many years of research, the transition mechanism is not clearly understood. In particular the growth mechanism of graphite from the liquid is still a subject of much debate.

The crystal lattice of graphite is hexagonal, with A-B-A-B stacking of semi-infinite hexagonal monolayers [17] (Fig. 5). The bonding is strong covalent in the plane of the layers and weak van der Walls between them as the large axial ratio, $c/a \approx 2.7$, indicates. Each monolayer is a 2-D polymeric graphene sheet [18] to which carbon atoms can attach easily in the monolayer plane (*a*-directions), but with a much lower probability normal to the monolayer (*c*-direction). The A and B layers are displaced by half of the *c*-axis spacing. Because of the difference in the bonding forces between the *a*- and *c*-directions, it is reasonable to assume that the

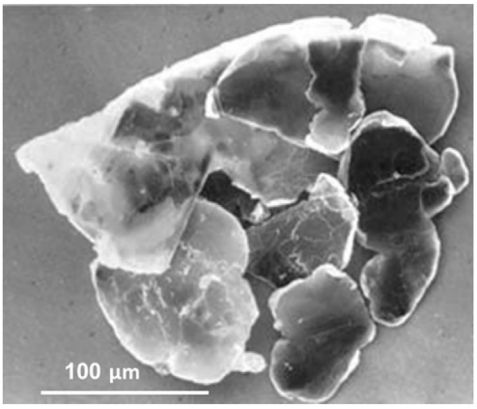

a) lamellar graphite– lettuce growth [1]

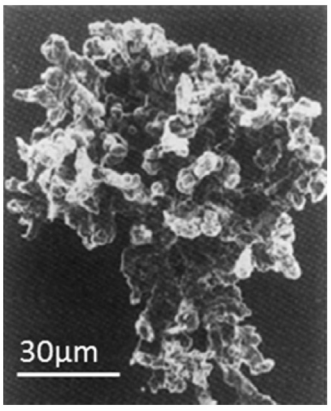

b) compacted graphite – cauliflower growth [2]

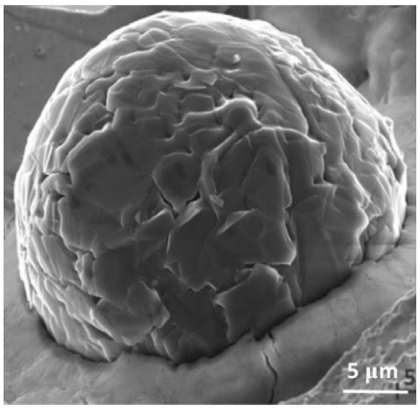

c) spheroidal graphite– cabbage growth [3]

Fig. 1. Typical graphite shapes obtained from commercial cast iron through deep etching and extraction.

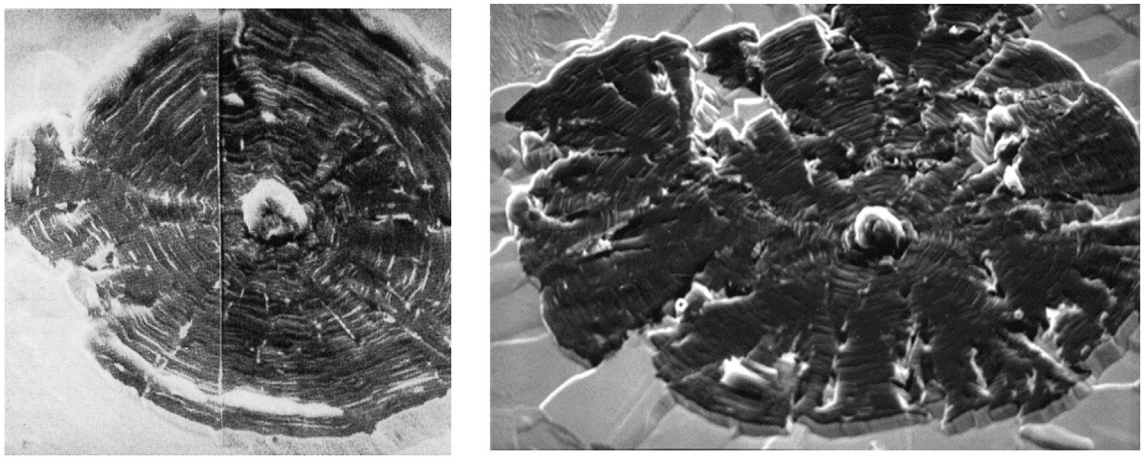

a) well-formed graphite spheroid [11] b) graphite spheroid with separated sectors [11]

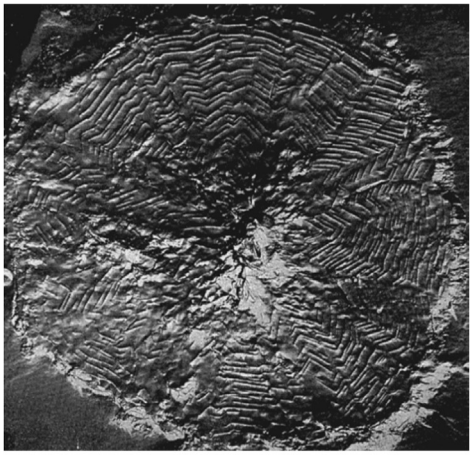

c) conical sectors with zig-zag steps, x2500 [4]

Fig. 2. SEM images of spheroidal graphite showing conical sectors.

preferred (normal) growth habit for graphite is in the *a*-direction, producing a sheet.

The growth of graphite in cast iron starts with the formation of 2-D one-atom thick layers of crystalline graphite (graphene sheets) that can grow easily in the *a*-direction. To produce a multilayer sheet (graphite lamella or plate), the graphene sheets will have to also grow in the *c*-direction. It was suggested [16] that, because surface-active impurities (S, O, N) are adsorbed at the unsaturated edges of a platelet, growth in the *a*-directions is partially inhibited, and growth in the *c*-direction becomes more probable. Thus, in LG iron that is relatively rich in O and S, the 3-dimensional (3-D) graphite plates grow in the crystallographic *a*-directions with the {0001} basal planes parallel to the plane of the lamellae and thicken in the *c*-direction.

Thickening of the platelets occurs through spiral growth at screw dislocation steps or by 2-D nucleation of the sheet in the *c*-direction. There is microscopy evidence for both (see for example Fig. 9 in Ref. [19] and Fig. 12 in Ref. [20]).

Graphite lamellae exhibit two types of defects: twin boundaries, which tilt the flake out of the basal plane, and twist boundaries (stacking faults) that lie on the basal planes (Fig. 6-a and -b). Twin boundaries defects may result in graphite branching through splitting along its basal plane while growing in the *a*-direction. Twist boundaries cause a rotation about the *c*-axis of the graphite. Based on experiments on Ni–C alloys, Double and Hellawell [21] suggested that successive layers are stacked together in one of three ways such that they are related by rotations of about 13°, 22° or 28° about the *c*-axis (Fig. 6-c). Thus, graphite lamellae are composed of layers of fault free crystal some 10^{-4} mm thick.

1.2. Effect of minor (impurity) elements

As experimental evidence demonstrates, the two main influences responsible for the changes in graphite morphology are the impurities in the melt (type and level) and the cooling rate of the alloy. The impurities affecting graphite growth can be divided in two categories:

a) reactive impurities favoring the LG-to-SG transition (Mg, Ca, Y and Lanthanides (Ce, La)), typically called compacting or spheroidizing

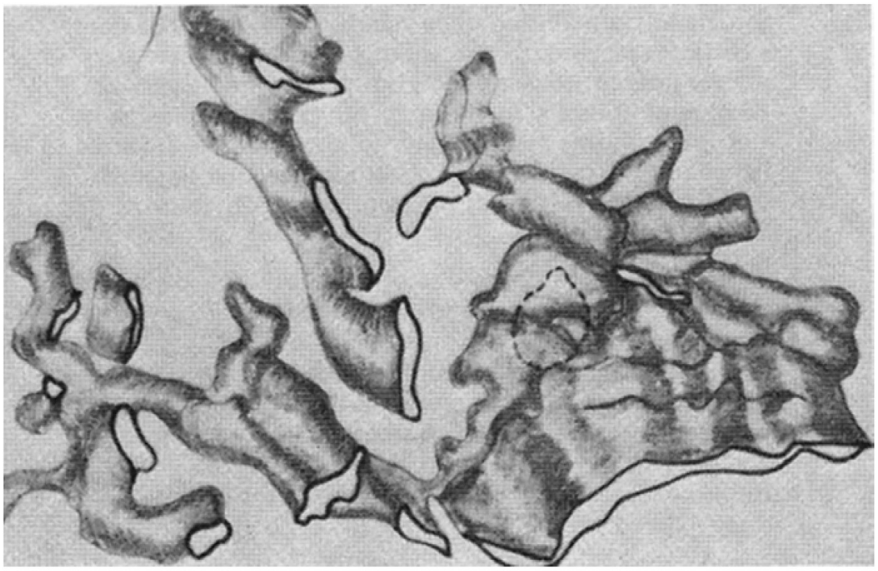

a) reconstructed through successive polishing [5]

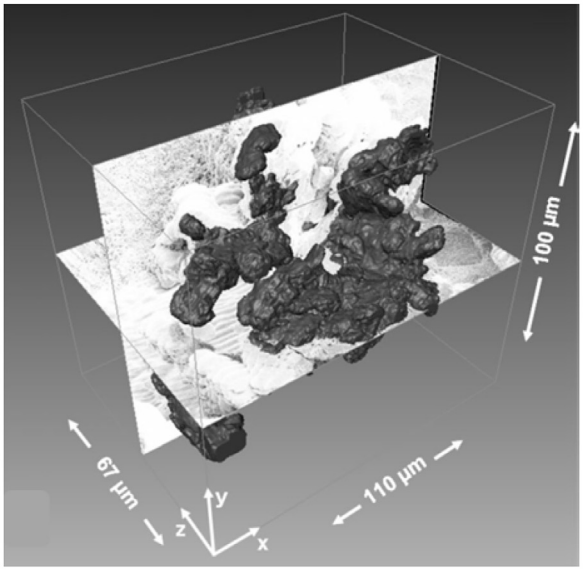

b) reconstructed through nano-tomography [6]

Fig. 3. Reconstructed images of compacted graphite aggregates.

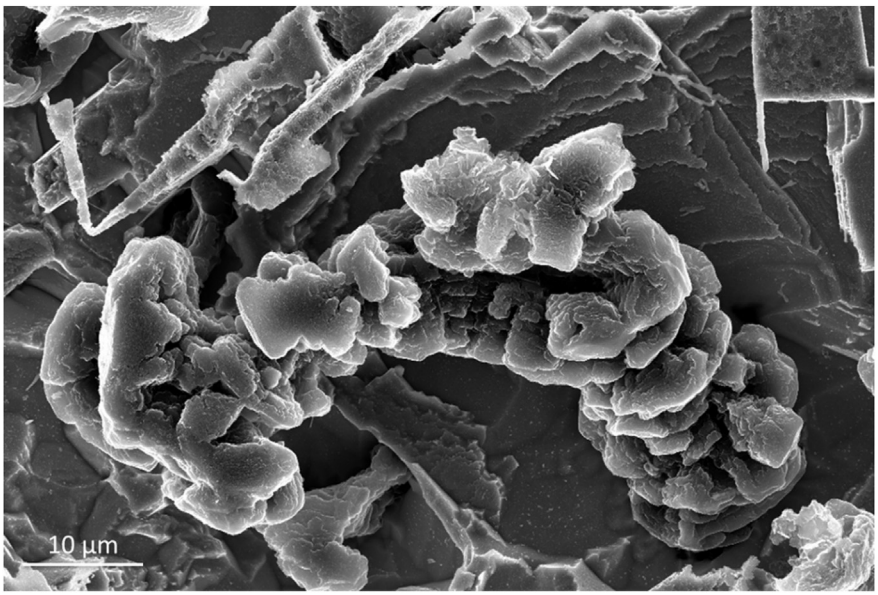

Fig. 4. SEM micrograph of deep-etched iron sample exhibiting chunky graphite.

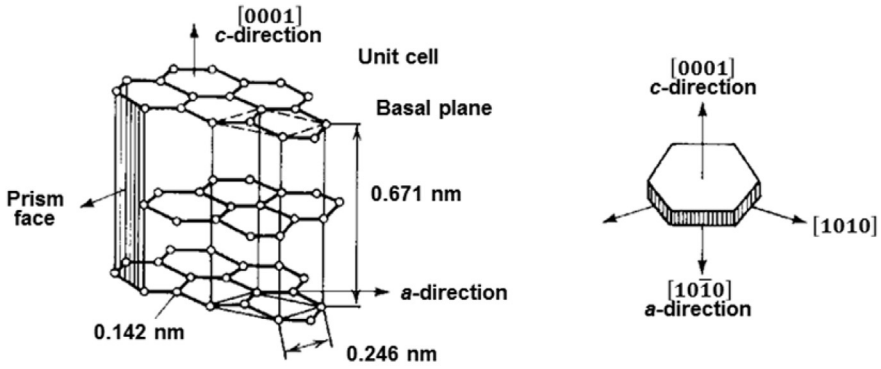

Fig. 5. Crystallographic structure of graphite.

b) surface-active impurities favoring the SG-to-LG transition (S, O, Al, Ti, As, Bi, Te, Pb, Sb) termed anti-compacting or anti-spheroidizing

It is well established that higher cooling rates, decreasing amounts of anti-compacting impurities, and increasing amounts of compacting impurities favor the transition LG-to-CG-to-SG.

All elements decrease the surface energy of liquid Fe–C alloys. However, while Ni, Cu and Si slightly reduce the surface energy, Ca, Mg, Ce, S, Se, and Te have a much stronger effect [24]. For example sulfur decreases the surface energy from 1.38 J/m^2 at 0.01%S, to 0.92 J/m^2 at 0.07%S [25]. Reactive impurities remove surface-active impurities generating high interface energy (*e.g.* 1.45 J/m^2 measured in Ref. [26]). Because in Fe–Mg alloys the interface energy γ_{Fe/Gr_prism} is higher than the γ_{Fe/Gr_basal} energy, while the opposite is true for Mg-free melts, McSwain and Bates [27] concluded that graphite grows from the melt normal to the plane with the lowest interfacial energy, which is the *c*-direction for the Fe–C–Mg alloys and the *a*-direction for the Fe–C–S alloys.

Auger analyses show concentrations of oxygen and sulfur in iron (but not in the graphite) adjacent to the metal-lamellar graphite interfaces, of about 20 at.% oxygen and 5 at.% sulfur in some two or three atomic layers [28]. Both S and Te segregate to the iron/graphite interface [29]. In the S doped alloys, LG was generally covered with a monolayer of S with patches of O in the form of iron oxide having a thickness on the order of 2 nm. Sulfur segregates to the iron/graphite interfaces from the liquid at the growth front, but O forms at these interfaces during the cooling.

1.3. Theories of graphite growth in cast iron

In Fe–C–Si alloys graphite can be produced through solidification, or through solid state transformation (heat treatment). The final morphology of graphite produced through the solidification route is the result of a four-stage growth process: from the liquid, during the eutectic transformation, during cooling to the eutectoid temperature, and during the eutectoid transformation. In this work we are only concerned with graphite obtained

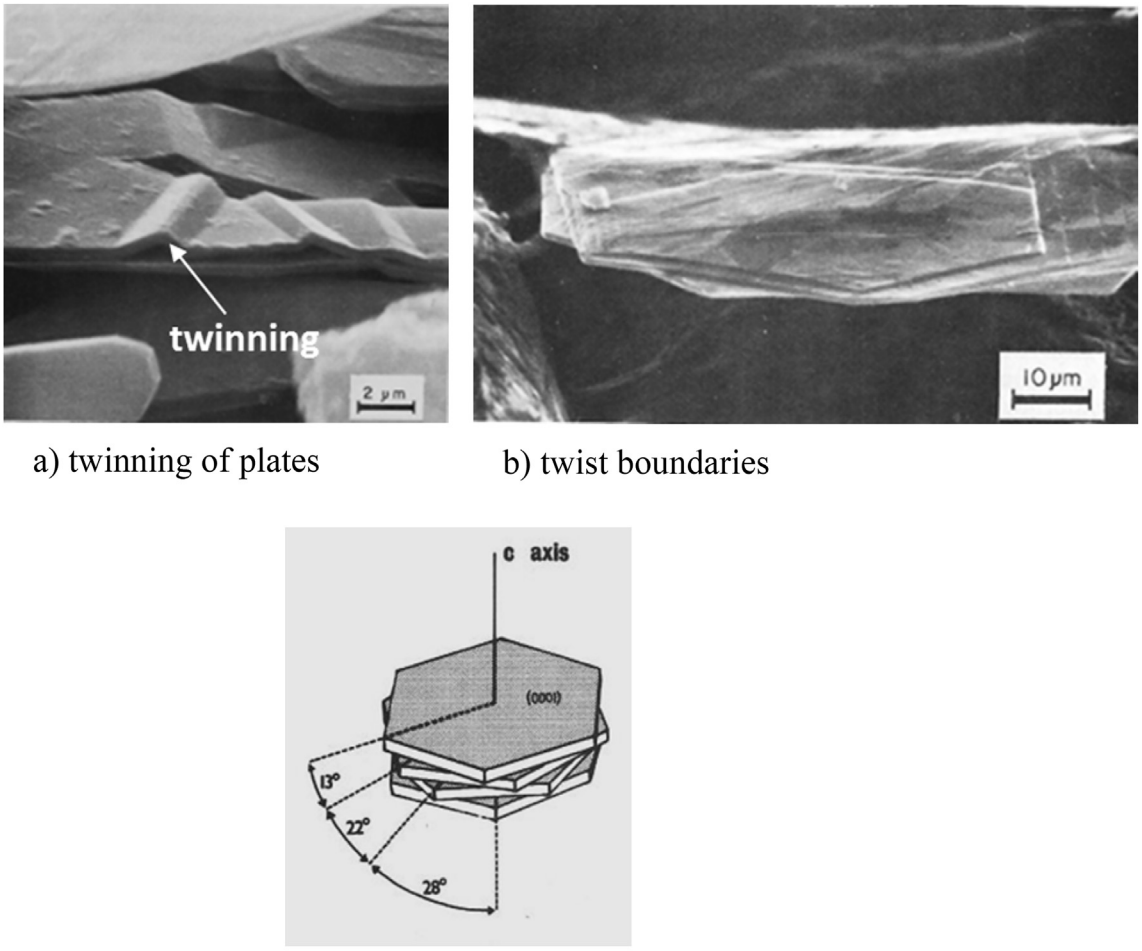

Fig. 6. SEM micrographs of defects in graphite [22], and schematic representation of *c*-axis rotational stacking faults [23].

through solidification. While graphite nucleation is particularly important in industrial processes, it will not be addressed in this work. The reader is referred to recent discussions on the subject [30,31].

Growth of lamellar graphite is fairly well understood, but that of compacted and spheroidal graphite and the transition LG-CG-SG are still the subject of much debate and in need of research. Some early concepts derived from SEM examination deep etched metallographic samples [32] are summarized in Fig. 7. Once nucleated, the LG/γ eutectic grain grows in a radial manner. The graphite lamellae are made of graphite sheets that bend, twist and branch, while growing in the *a*-direction. A reorientation of the graphite sheets occurs when transiting to CG, giving the appearance of growth along the *c*-axis. After losing contact with the liquid the tip of CG may grow as a spheroid.

Den et al. [33] suggested a similar model in which the transition from LG to CG or from SG to CG is based, as in the previously discussed model, on changing of the growth direction of the graphite aggregate form *a*- to *c*-direction, or from *c*- to *a*-direction (Fig. 8). However, while the artistic rendition is correct, none of these models provides a plausible explanation of the extensive growth in the c-direction and of the occurrence of radial sectors in SG.

Chunky graphite is a degenerated form of spheroidal graphite reported as early as 1970 [34]. It grows as a highly branched, interconnected form of graphite producing a generally spherical eutectic grain with the same radial structure as spheroidal graphite. The dominant growth is along the c-axis of the graphite crystal. Liu et al. [11] proposed the growth model in Fig. 9, where chunky graphite is characterized by a series of clustered, sector-shaped graphite segments.

Many theories have been proposed over the years to describe the mechanisms of formation of various graphite shapes, and reviews of these theories have been periodically written, *e.g.*, ref. [35–37]. One point of agreement is that graphite shape transitions in cast iron are the effect of growth kinetics modified by the adsorption of surface active elements (S, O) at the growth sites.

The role of the reactive (Mg, Ce, La) and surface active elements (S, O, Pb, Sb, Ti.) has been recognized early in a theory by Herfurth [38] that postulates that the change from lamellar to spheroidal graphite occurs because of the change in the ratio between the

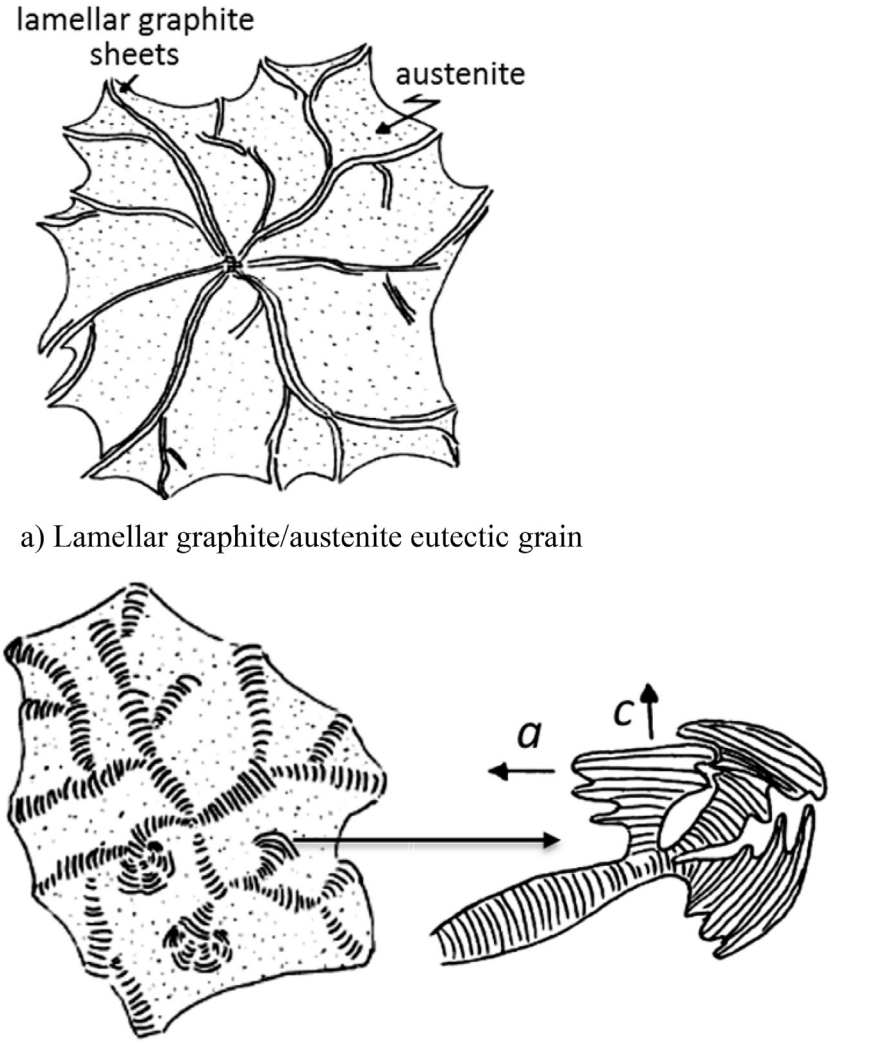

Fig. 7. Schematic representation of LG and CG eutectic grains [32].

growth velocity on the $[10\bar{1}0]$ face (a-direction) and growth on the [0001] face of graphite (c-direction).

The significant change in surface energy caused by the addition of reactive elements prompted a number of investigators to conclude that the higher surface energy promotes spheroidal graphite as the system attempts to decrease its energy. According to DeSy [39] and Buttner et al. [40] there is a critical graphite/liquid (Gr/L) interface energy above which polycrystalline SG is favored over single-crystal LG. This theory was supported by many investigators, *e.g.* [25,28,41–43]. However, if a crystal becomes larger than 1 μm the change in free energy because of departure from equilibrium becomes small compared with the super-saturation necessary for crystal growth [44].

In the growth model proposed by Sadocha and Gruzleski [14] a graphite spheroid may result from repeated bending of the graphite sheets. A large number of steps on the surface of the spheroid are assumed to grow in the a-direction by curved crystal growth, with

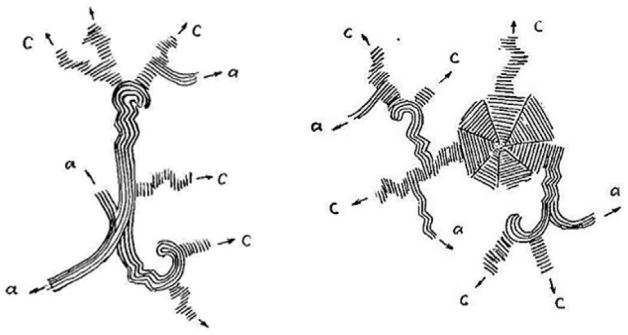

Fig. 8. Schematic representation of growth of compacted graphite [33].

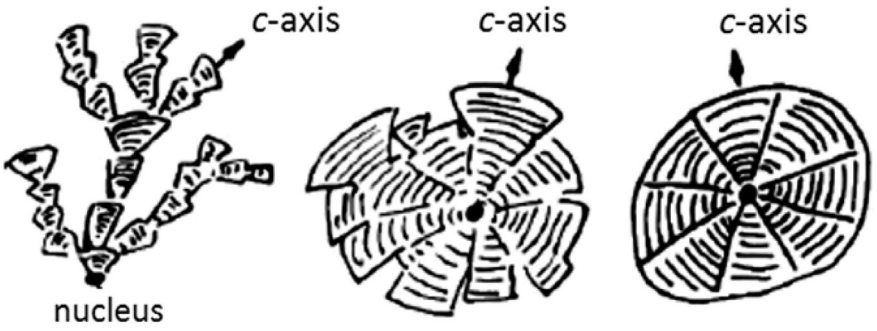

Fig. 9. Schematic representation of the growth patterns of chunky graphite (left), an imperfect graphite spherulite (middle), and spheroidal graphite (center) [11].

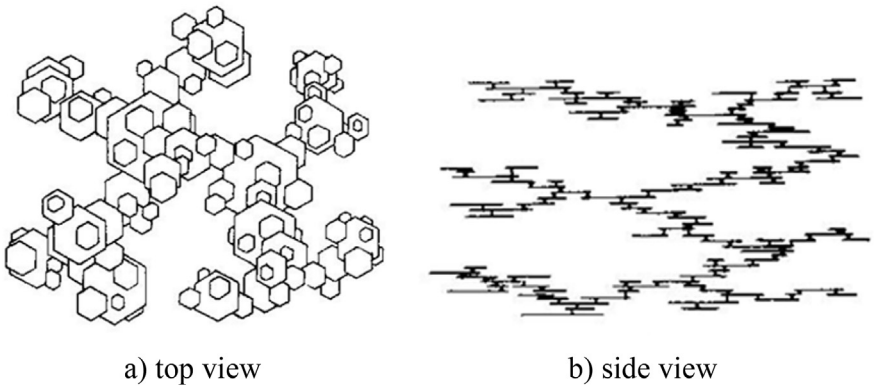

Fig. 10. A foliated dendrite [46].

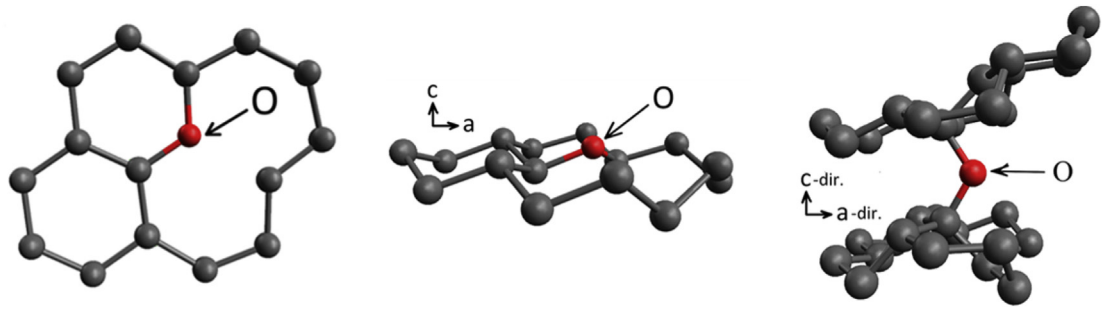

Fig. 11. Growth of graphene in the c-direction, caused by the attachment of oxygen out of the basal plane, and carbon-ring defects (Avogadro software). Pentagonal rings create curvature in the basal plane, which can cause conical or spheroidal growth of graphite [49].

Table 1
Chemical composition (mass%) of alloying additions and melt treatment alloys.

Alloying addition	Si	Mn	Mg	Lanthanide	Ca	Al	C	Ti	Zr	Ba	Others	Fe
Fe75Si	74.6				0.3	0.7						bal.
Fe75Mn	2.13	74.8					5.49				0.08P	bal.
Graphite							98.9				0.03S	–
Fe72Ti						4.5		72.3				bal.
FeSiMg	47.2	0.30	6.02	0.88	1.15	0.24						bal.
Inoculant	62.6	5.96	0.22	<0.07	1.79	1.01		0.13	6.77	0.65		bal.

Table 2
Chemical composition (mass%) of experimental cast irons.

Series	Graphite	C	Si	CE	Mn	P	S	Mg	Others
Q1LG	LG	3.07	1.91	3.65	0.57	0.014	0.011	<0.01	0.014Ti
Q2SIG	LG, SIG	2.94	1.92	3.50	0.58	0.022	0.011	<0.01	0.18Ti
Q3SIG	SIG	3.10	1.85	3.64	0.53	0.021	0.011	<0.01	0.32Ti
Q4CG	LG, SG	3.77	2.23	4.44	0.14	0.015	0.015	0.013	0.021Ti
Q5CG	CG, 20%SG	3.68	2.14	4.32	0.14	0.016	0.014	0.020	0.021Ti
RT1LG	LG	3.36	2.17	4.06	0.51	0.033	0.082	–	0.2Cr, 0.04Sn, 0.27Mo
RT2CG	CG	3.74	2.26	4.44	0.28	0.028	0.001	0.008	Lanthanides n.m.
RT3ChG	chunky	3.72	2.09	4.38	0.12	0.033	0.012	0.052	0.002Sb, 0.005Sn, 0.006La

SIG: superfine interdendritic graphite; SG: spheroidal graphite; CG: compacted graphite.
CE: Carbon Equivalent calculated as %C + 0.31·%Si + 0.33·%P-0.027·%Mn + 0.4·%S.
n.m: not measured.

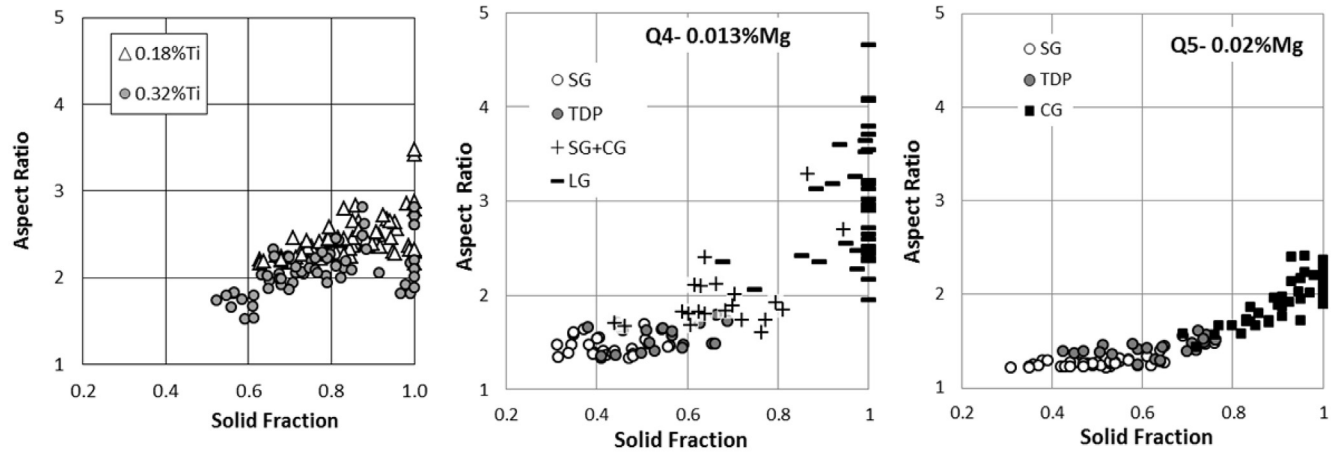

a) Q2SIGr – 0.18%Ti and Q3SIGr – 0.32%Ti

b) Q4CG - 0.013% Mg

c) Q5CG - 0.02% Mg

Fig. 12. Graphite shape as a function of fraction solid and chemical composition.

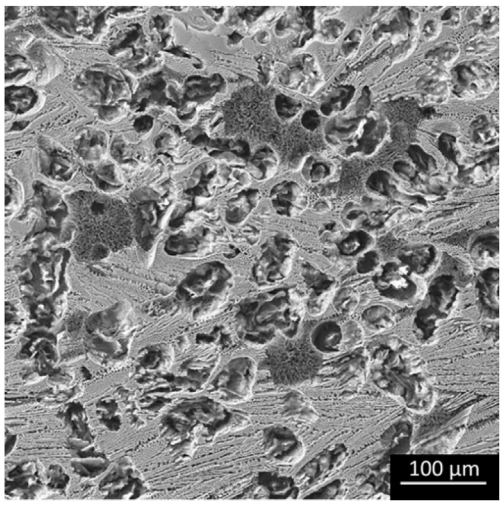

a) no Mg: graphite growth at the γ/L interface

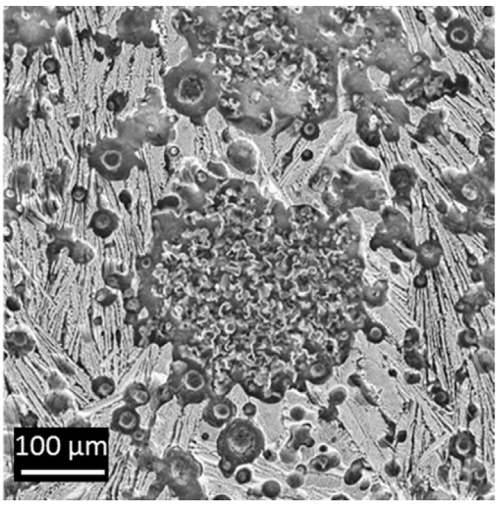

b) 0.013% Mg iron: SG and curly graphite

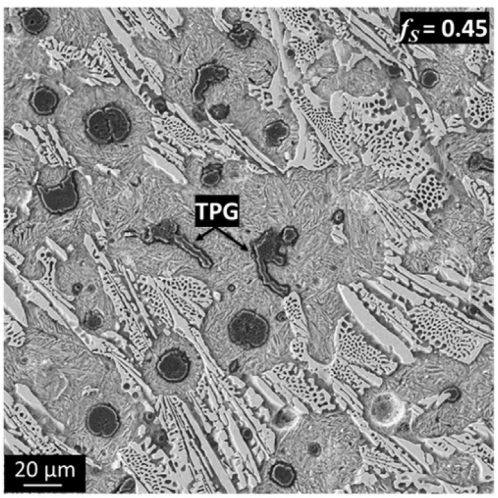

c) 0.02% Mg iron: SG and TPG

Fig. 13. Low magnification SEM micrographs of early solidification from interrupted solidification experiments.

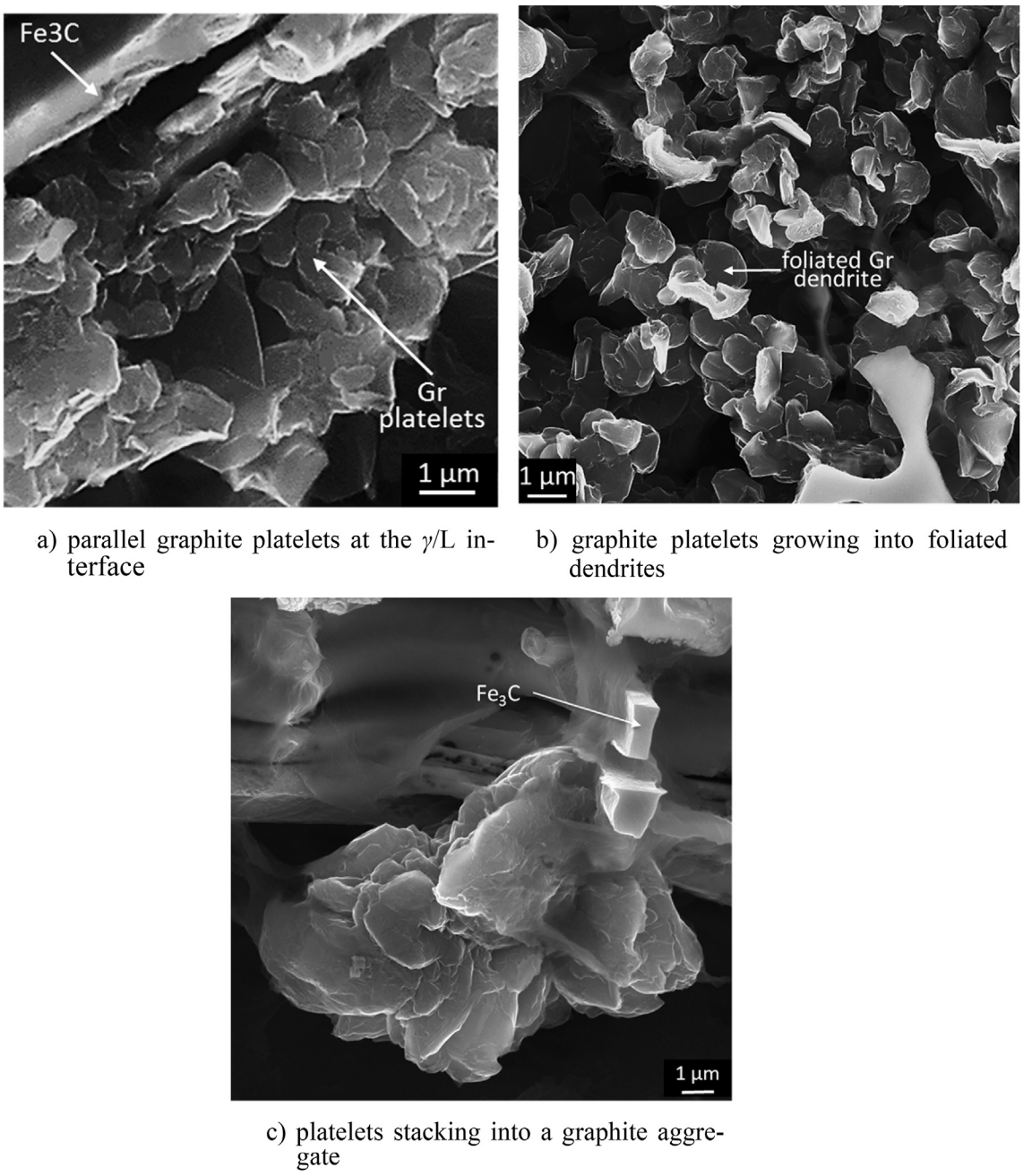

a) parallel graphite platelets at the γ/L interface

b) graphite platelets growing into foliated dendrites

c) platelets stacking into a graphite aggregate

Fig. 14. SEM images of interrupted solidification of low-sulfur LG irons ($f_S = 0.64$, heat Q1LG) showing graphite growing at the γ/L interface in contact with the liquid (Fe_3C).

the low energy basal plane of graphite exposed to the liquid. In the presence of surface-active impurities that decrease the surface tension (S or O), the spherical shape is deteriorated into a lamellar one.

According to Double and Hellawell [16,23], the ability of a graphene sheet to bend in steps of 20°45′ about three ⟨1100⟩ axes mutually inclined at 120° makes it possible for a lamellar crystal to grow into an incoherent spherical form, or alternatively, to roll upon itself as conical helices through a conical dislocation mechanism.

The role of the growth velocity ratio in the a- and c- direction in determining the graphite shape has also been advocated by Amini and Abbaschian [3], although not based on surface energy arguments, but on kinetic ones. Attempting to explain the occurrence of SG in hypereutectic Ni–3%C alloys solidified at very high cooling rate (quenching), they argued that a roughening transition from faceted to diffuse Gr/L interfaces is responsible for the LG-to-SG transition. They argued that the growth in length (a-direction) of LG is diffusion controlled, while the thickening (c-direction) is surface controlled through 2-D poly-nucleation growth. Further they assumed that at small solidification rates, the graphite crystals basal and prismatic planes are faceted. As the interface velocity increases, the supersaturation increases and the faceted interface becomes gradually rough. At intermediate rates the prismatic interfaces become rough and grow faster, while the basal plane remain faceted, leading to the formation of LG. At high growth rates

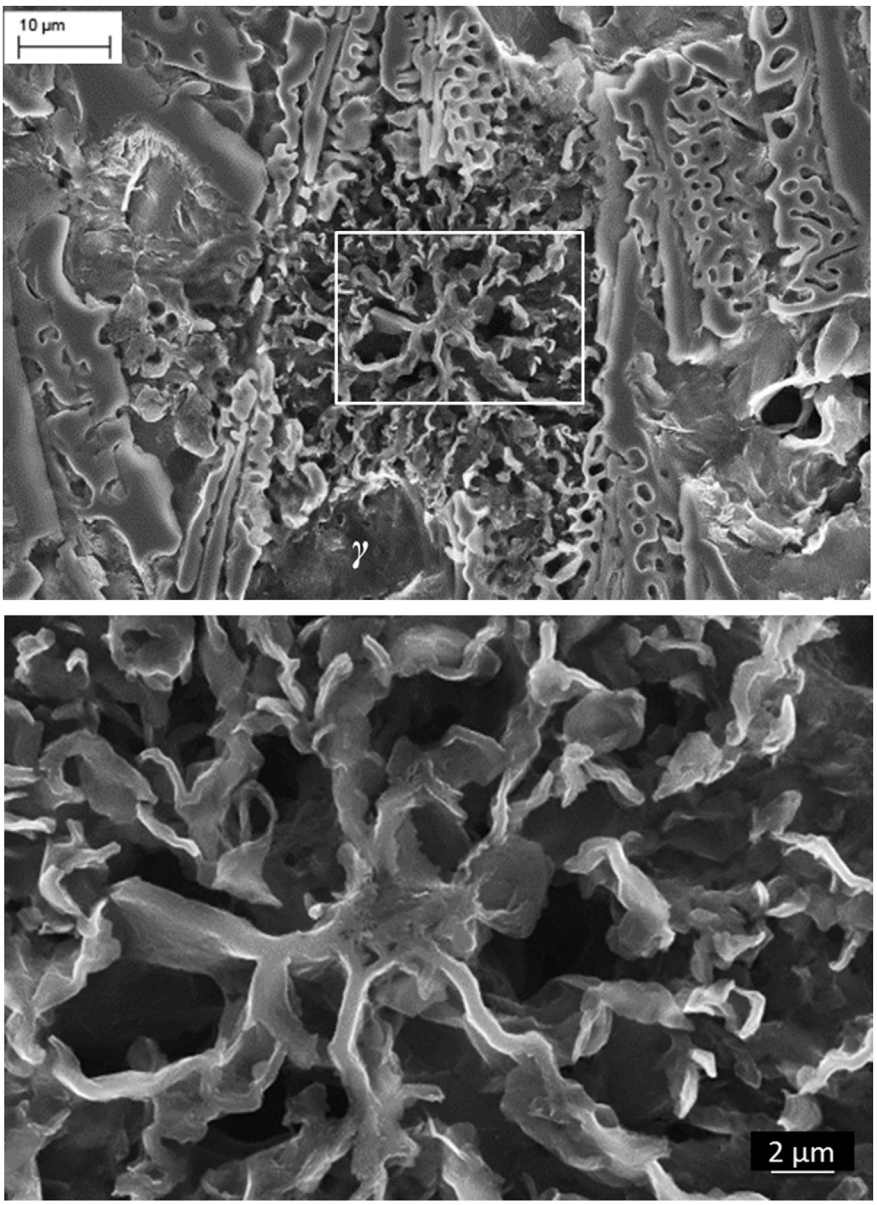

Fig. 15. SEM images of interrupted solidification of low-sulfur LG irons ($f_S = 0.55$, heat Q1LG) at two magnifications: radial growth of graphite plates.

both interfaces grow with similar velocities, resulting in "bulky" spherical morphology.

More recent transmission electron microscopy work motivated Theuwissen et al. [45] to contend that graphite precipitates consists of growth blocks stacked upon each other, and that graphite crystals develop mainly by a 2-D nucleation and growth mechanism. Yet, unlike the layer by layer growth, in which each new layer corresponds to a graphene sheet advocated by Amini and Abbaschian, they argued that there should be a critical block thickness required for further growth of graphite precipitates instead of atomic layers.

While studying the growth of hexagonal platelets of cadmium iodide (CdI_2) crystals, Saratovkin [46] noticed that under certain conditions the platelets develop into dendrites. He then proceeded to postulate a growth mechanism producing "foliated crystals", which are assemblies of thin plates separated by solvent impurity layers, and "foliated dendrites" (Fig. 10). This concept was then used to explain graphite growth in cast iron and the entrapment of iron between the foliated graphite plates. Growth of iron carbide in cast iron was also considered to be a case of foliated crystals.

Examining high magnification SEM photographs, Roviglione and Hermida [20] noted that the constitutive elements of CG and SG are clusters of randomly distributed and heavily distorted small faceted crystals, with basal planes forming major surfaces, and prismatic planes forming minor ones, also confirmed by diffraction studies. They reasoned that these are foliated dendrites, as termed by Saratovkin, They further argued that addition of reactive elements produce compaction forces on the graphite by the austenite shell and the melt, and cause increased twinning of the foliated dendrites, resulting in the crystallization of CG or SG.

Comprehensive observations on carbon nano-fibers using SEM, TEM, STM, and XRD revealed that a diversity of macroscopic morphologies can be obtained by stacking two types of structural units, carbon nano-rods or carbon nano-platelets [47]. A carbon nano-rod

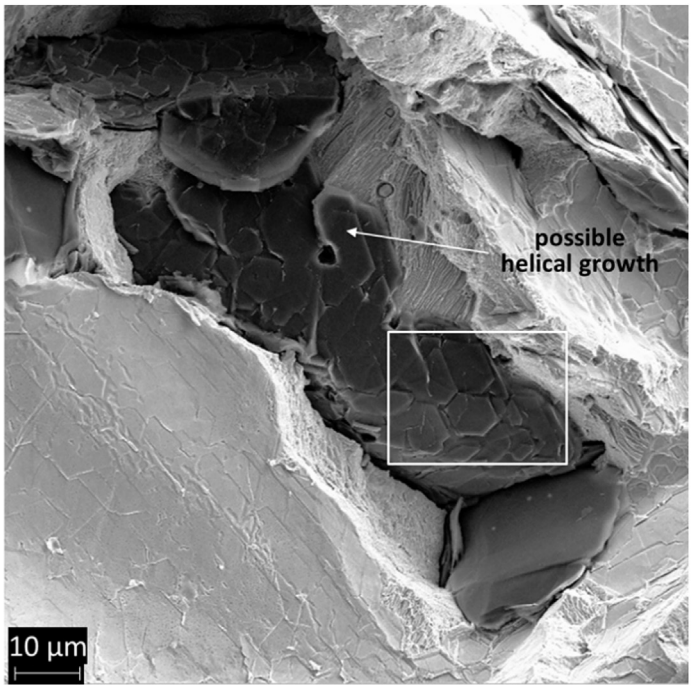

a) fracture surface exhibiting the substructure of a graphite lamella

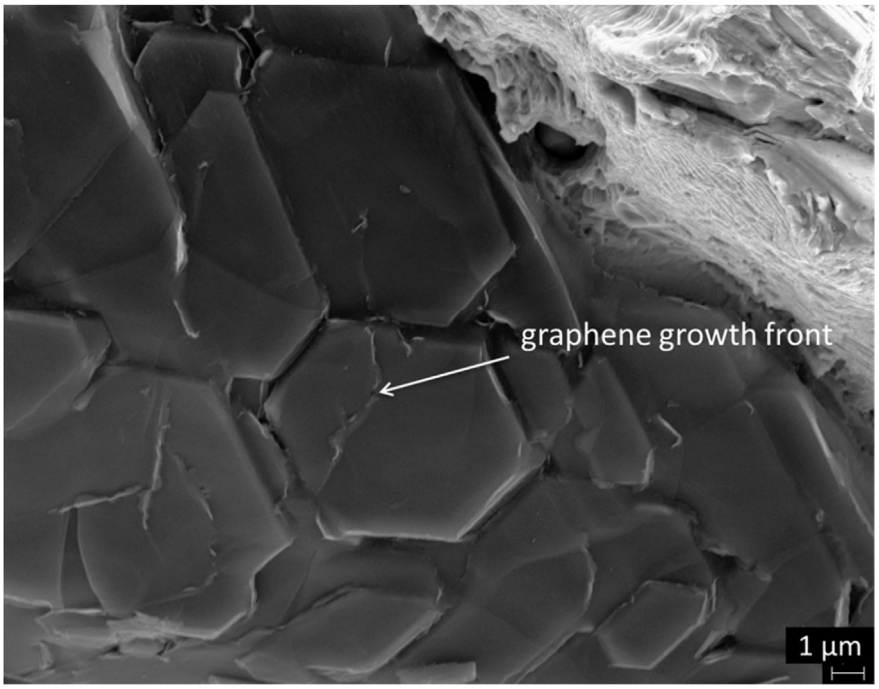

b) higher magnification of the microstructure in (a)

Fig. 16. SEM micrographs of fracture areas in fatigue fractured lamellar graphite iron (sample RT2) [Compliments of W.L. Guesser and the Tupy/SENAI project].

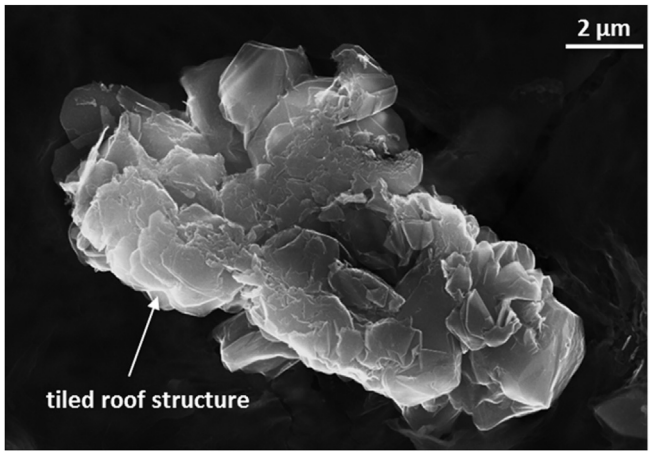

Fig. 17. SEM image of early solidification Ti-modified graphite from sample Q3SIG (0.32% Ti).

is a carbon cluster of 8–10 graphene layers with diameters of about 2.5 nm and lengths of 15–100 nm. Carbon nano-platelets appeared to be sets of 5–25 graphene stacks with dimensions of 2.5 nm thick, and 10 × 32 nm surfaces. Recently, the authors of this paper identified the existence of thin graphite platelets as the building blocks of both spheroidal and compacted graphite [48], confirming the statement of Roviglione and Hermida. The surface dimension of the platelets was typically of the order of 1 μm, which is about an order of magnitude higher than the carbon nano-plates.

Muhmond and Fredriksson [49] analyzed the effect of substitution of various elements in a monolayer of graphene. Simulations with a molecule editor program and visualizer (Avogadro software) established that trace elements in the melt can attach to the basal plane of a graphite crystal and that pentagonal, hexagonal, and high-order carbon-rings can be present as defects in the basal plane. They concluded that in the absence of all types of defects graphite crystals grow mainly in the a-direction. However, the presence of some trace

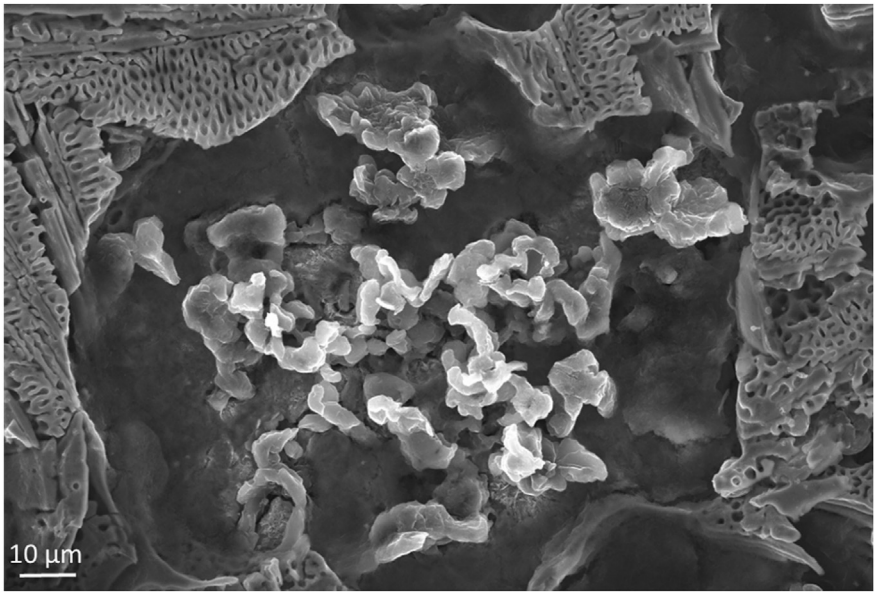

a) $f_S \cong 0.45$

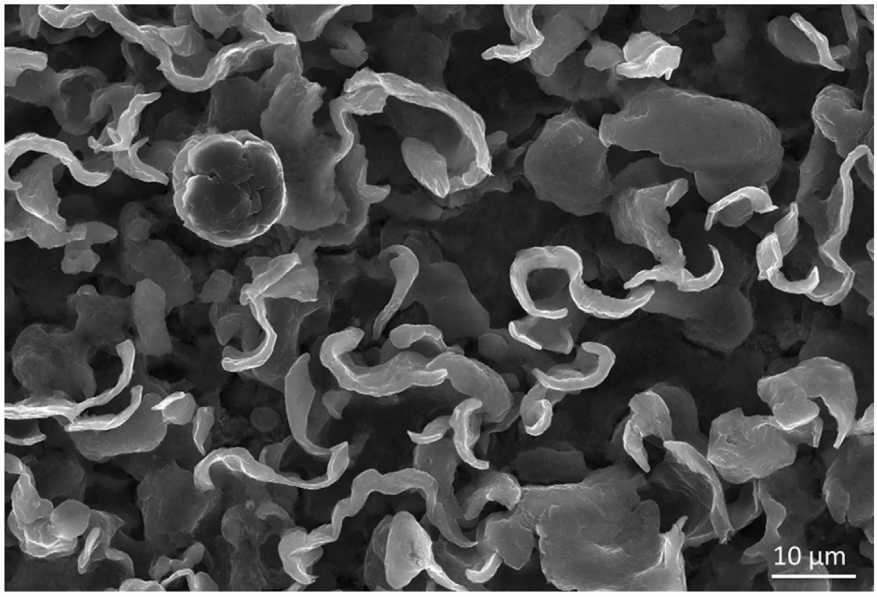

b) $f_S \cong 0.65$

Fig. 18. SEM images of early solidification Mg-modified graphite from sample Q4CG (0.013% Mg) at two fraction solid: curly graphite.

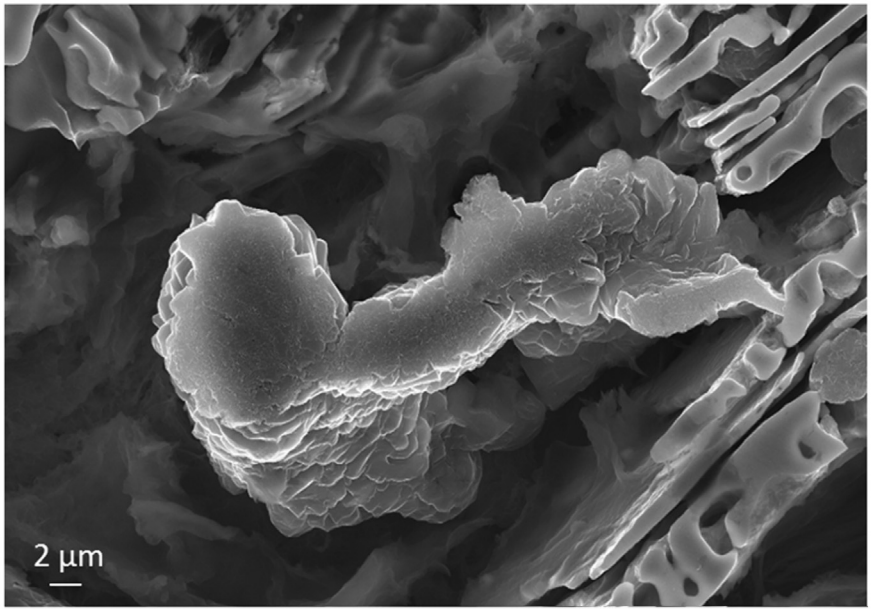

a) tadpole graphite

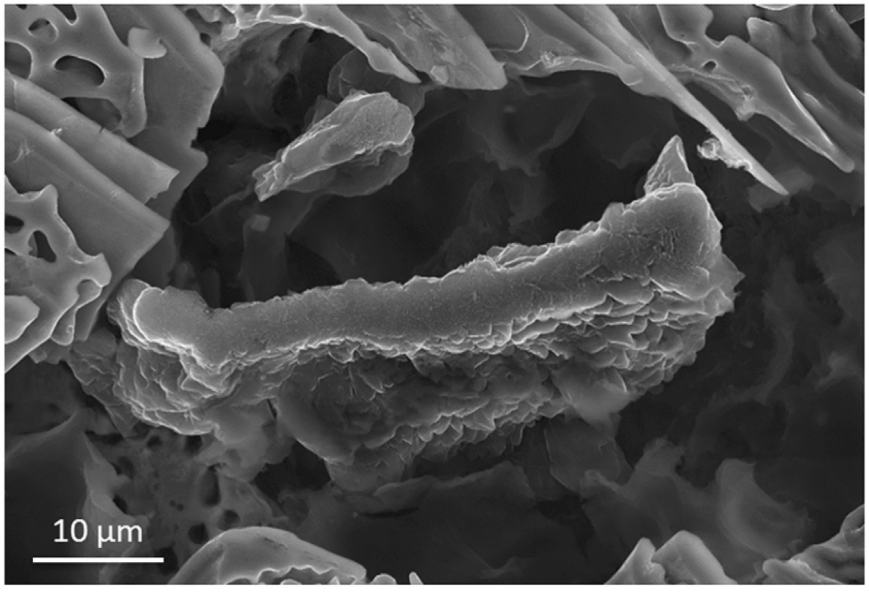

b) compacted graphite

Fig. 19. SEM images of early solidification Mg-modified graphite from sample Q5CG (0.02% Mg).

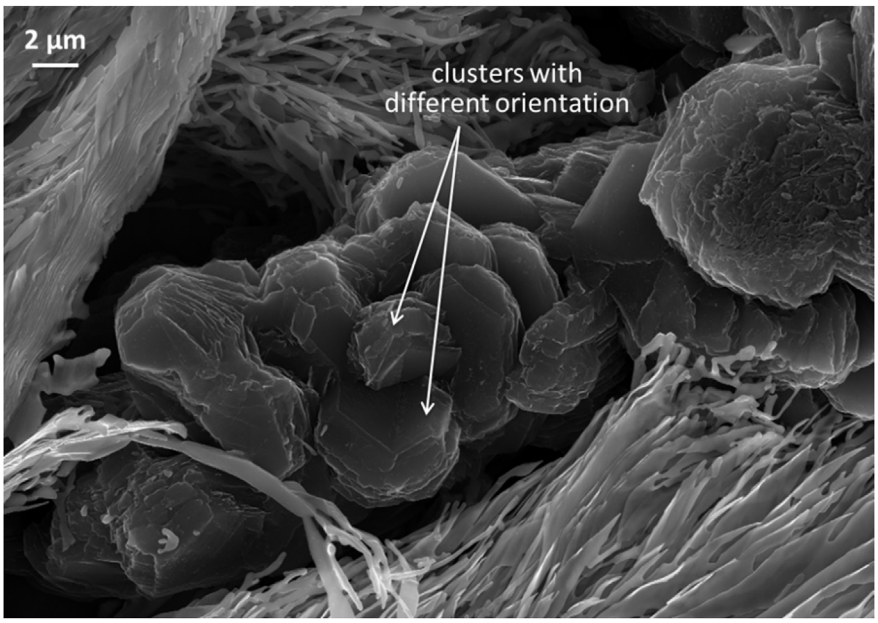

Fig. 20. SEM image of CG in deep etched 0.013% Mg iron: clusters of graphite platelets with different orientations forming blocky graphite.

elements, vacancies, and carbon-ring defects creates situations for growth along the c-direction, and/or curvature in the basal plane, as exemplified in Fig. 11 for oxygen. Nitrogen behaves similar to oxygen. Other elements, such as S, Se, and B, attach to the basal plane and stabilize lamellar growth. These conclusions are in line with Double and Hellawell's suggestions [16].

From this analysis it follows that there is a wide range of folding and wrapping possibilities for the graphene sheets which could describe the many graphite morphologies encountered in industrial cast irons. The lamellar and spheroidal forms of graphite may be regarded as two extremes. Other intermediate graphite shapes, such as compacted graphite, are the result of mixed growth mechanisms.

The goal of this work was to investigate the crystallization of graphite from liquid multicomponent Fe–C melts from experimental evidence obtained during early solidification through interrupted solidification experiments, and to integrate this new information in the body of knowledge on the mechanism of graphite morphology formation in industrial multicomponent Fe–C melts.

2. Research approach

The material for in-depth SEM analysis of graphite morphology was obtained from laboratory Fe–C–Si melts of commercial composition with low sulfur content and various amounts of titanium and magnesium. The compositional range was designed such as to include irons with graphite ranging from lamellar type-D (LG), to superfine-interdendritic (SIG), and to compacted (CG). Two series of test samples were used in this research: 1) samples obtained from quenched (interrupted solidification) thermal analysis cups, notation Q; 2) samples obtained from industrial iron castings (room temperature, notation RT).

2.1. Melting and casting of the quenched-series samples

For the interrupted solidification experiments, five melts were produced in a 100 kg medium frequency induction furnace (250 Hz, 100kw). For the first three melts (Q1LG, Q2SIG and Q3SIG) the charge consisted of 37 kg of ductile iron returns and 13 kg of high purity pig iron. To adjust the composition, ferro-silicon (Fe75Si), ferro-manganese (Fe75Mn), and commercial graphite additions were made to the melt as needed. The melts had three levels of titanium, 0.014%, 0.18% and 0.32%, which was added as ferro-titanium (Fe72Ti). The compositions of the melt additions are given in Table 1. After superheating to 1500 °C, the iron was transferred into the pouring ladle.

For the following two melts (Q4CG and Q5CG) the charge consisted of 20 kg of ductile iron returns, 32 kg of high purity pig iron, 1.3 kg of graphite and 0.3 kg of Fe75Si. Carbon and silicon composition corrections were made after melting as needed. After superheating to 1500 °C, the iron was transferred into the pouring ladle. To obtain compacted graphite with different levels of nodularity, FeSiMg alloy was deposited on the bottom of the ladle, as follows: 0.3% for Q4CG, and 0.4% for Q5CG.

From each melt six standard thermal analysis cups (36 × 36 × 43 mm) were poured and the cooling curves were recorded. Inoculation was performed by adding 0.2% of a commercial inoculant in each cup.

For five cups in each series, the solidification was interrupted by quenching in brine (to increase the thermal conductivity) at increasing times, to provide information on the microstructure at various stages during solidification. After cooling to room temperature, the cups were sectioned and prepared for metallographic examination.

The chemical composition of all samples and the room temperature overall graphite morphology is given in Table 2. For the Q-series, in addition to the elements listed in the table, the alloys contained 0.04%Cr, 0.01%Mo, 0.04%Ni, 0.04%Cu, and less than 0.01% Al.

2.2. Characterization

The fraction of the area occupied by the solid on the interrupted solidification samples was measured through quantitative metallography techniques on color and Nital etched samples, as

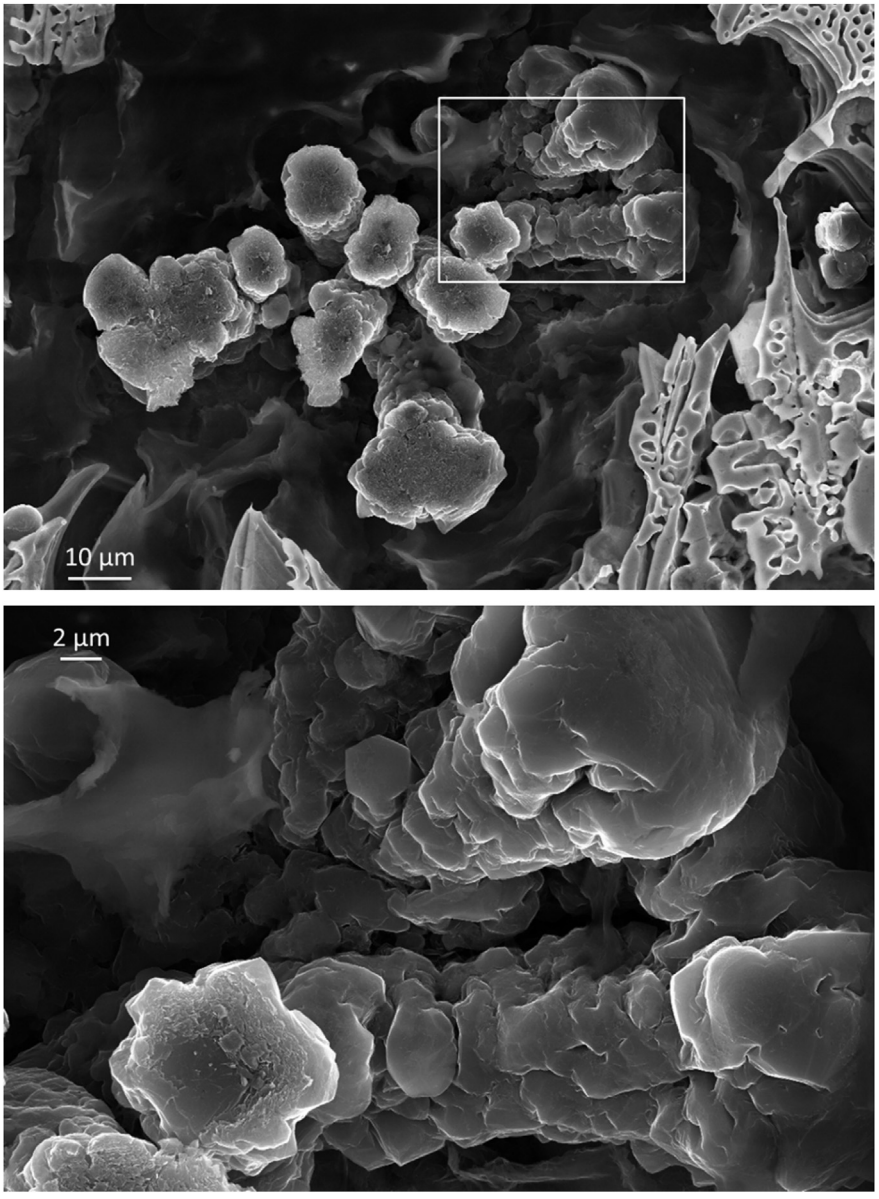

Fig. 21. SEM images of early solidification Mg-modified graphite from sample Q5CG (0.02% Mg): chunky graphite at two magnifications.

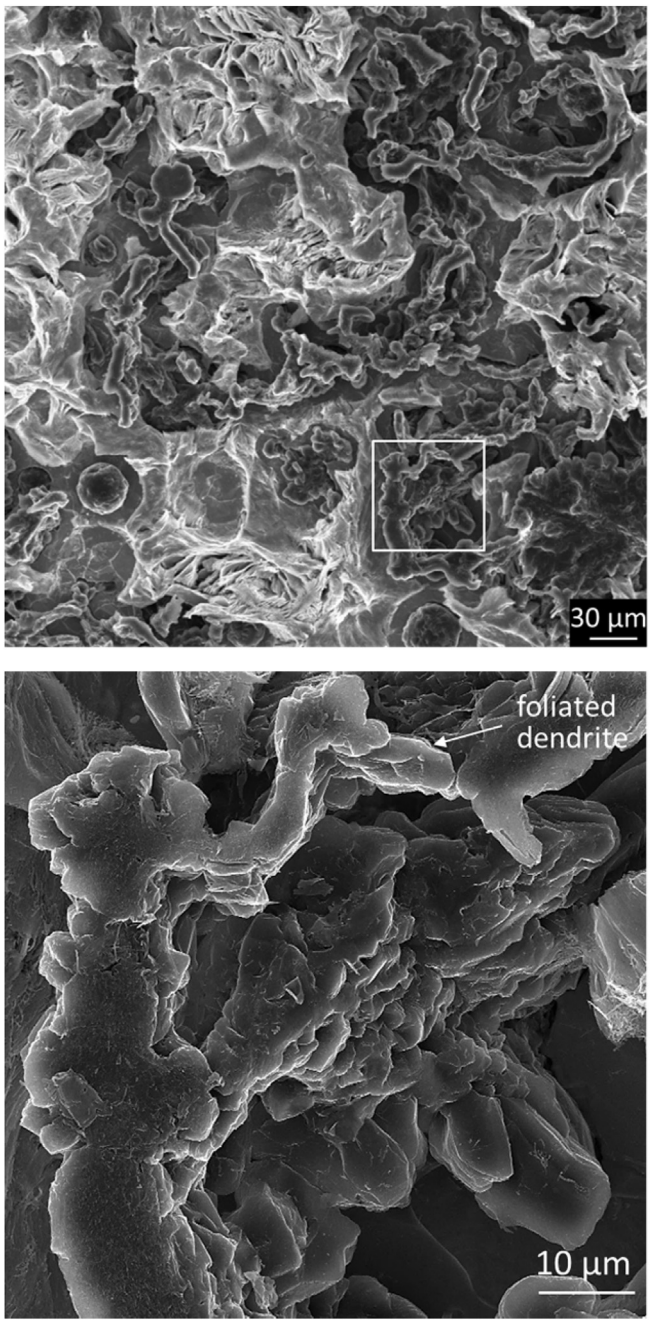

Fig. 22. SEM images of deep etched room temperature samples from series RT2CG at tow magnifications: foliated dendrites and branching of the CG dendrite.

described in detail in Ref. [50]. From each cup several horizontal sections samples were cut. As the cooling rate increases from the outside to the center of the cup, different fractions solids were obtained from the same cup.

The graphite shape was evaluated through quantitative metallography with the software Image J. While several graphite shape parameters such as roundness and sphericity were measured, only the aspect ratio *(AR = major_axis/minor_axis)* will be discussed here.

To reveal the morphology of the graphite the metallographic samples were deep etched to remove the matrix, as described in detail in a previous publication [51]. The deep-etched samples were then examined with an Ultra PLUS Carl Zeiss SMT with 0.8 nm resolution at 30 kV in the STEM mode. An X-Max 20 Oxford Instruments EDS detector with a resolution of 127ev/mm^2 was used to determine the local chemistry of inclusions and graphite nuclei.

3. Research results

3.1. Graphite shape

The evolution of graphite shape during solidification can be summarized through the graphs describing the change in aspect ratio as a function of the measured solid fractions, presented in Fig. 12 for the Q-series samples. In all instances the aspect ratio increases as solidification advances and as the fraction solid increases. It should be noted that the fraction solid depends on two variables: the cooling rate which increases from the center of the cup to its periphery, and the time of quenching after the beginning of solidification. The general graphite shape descriptors, SG, TPG, CG and LG on Fig. 12, imply that at room temperature the majority of the graphite was of this shape. A sample was marked as having TPG, as soon as tails were observed on graphite spheroids. This was considered to be the beginning of the transition from SG-to-CG.

In the Mg-free low-S iron, graphite grows in contact with both the austenite dendrites and the liquid (Fig. 13-a). Increasing the Ti level generates a more compact graphite, as demonstrated through Fig. 12-a for Ti levels of 0.18 and 0.32%, promoting the transition from interdendritic LG to SIG. When Mg was added to the iron, solidification started with graphite spheroids (Fig. 12-b,-c and Fig. 13-b). At about 0.4 fraction solid (f_S) some of the graphite spheroids exhibited one or more tails (Fig. 13-c). This is the so-called tadpole graphite (TPG) [52]. The graphite spheroids are surrounded by austenite, while tadpole graphite was in most cases connected to cementite, suggesting growth in contact with the liquid.

3.2. Graphite growth from the liquid

As described in an earlier paper [51], crystallization of graphite in low-sulfur, Mg-free iron, occurs at the γ/L interface. Initial growth of graphite takes place as parallel platelets in contact with the liquid (Fig. 14-a). The platelets, which are the building blocks for the graphite lamellae, are very thin, have micrometer-size width, and grow along their *a*-axis. The growth morphology is consistent with that of foliated dendrites (Fig. 14-b). The graphite platelets will then stack into aggregates (Fig. 14-c). If there is enough room between the austenite dendrites, quasi-spherical graphite aggregate in contact with the quenched liquid (carbides) and the austenite (γ) may grow, as shown in Fig. 15. Growth of the graphite plates (lamellae) occurs from the center in radial dendritic manner. The plates develop twins and branch as they grow. Such twins were noted in recent TEM work on a graphite lamella [53].

High magnification SEM examination of lamellar graphite in the room temperature sample RT2 (Fig. 16) reveals the substructure of the graphite plates (lamellae). The building blocks appear to be hexagonal platelets of 5–10 μm size (but at times larger or smaller) stacked along the *c*-direction, forming the "tiled roof" structure of a foliated crystal. The orientation of the "tiled roof" structure indicates the growth direction of the lamellae, which is along the *a*-direction of the platelets.

Titanium additions produce more compact graphite. This is seen on Fig. 12-a. The average aspect ratio at the end of solidification is 2.77 for the 0.18% Ti, and 2.44 for the 0.32% Ti samples. The substructure of Ti modified graphite still exhibits the tiled-roof structure, but the graphite platelets are smaller of the order of several

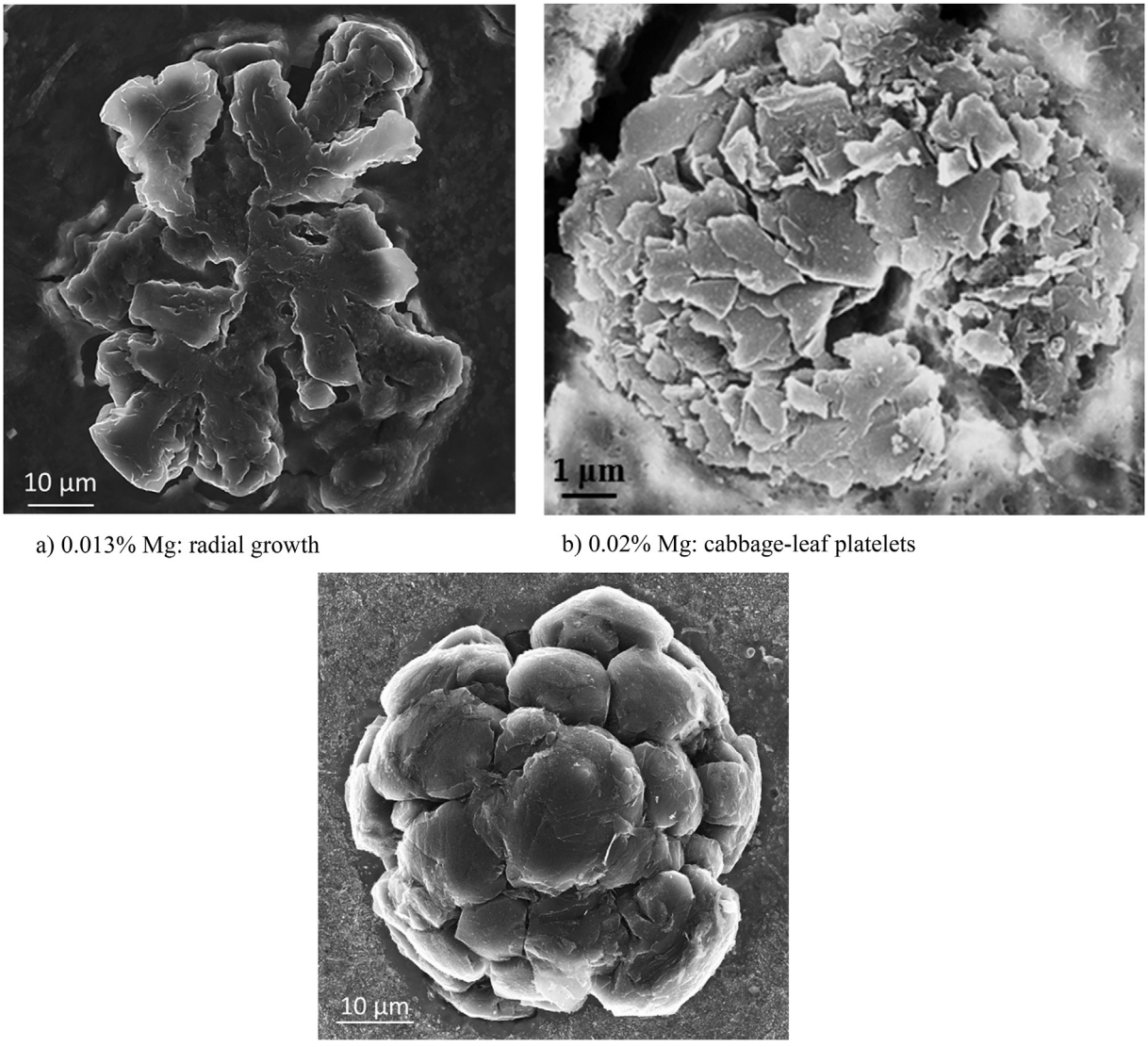

a) 0.013% Mg: radial growth

b) 0.02% Mg: cabbage-leaf platelets

c) 0.02% Mg: conical sectors

Fig. 23. Deep-etched SEM images of graphite spheroids precipitated at $f_S < 0.4$ in Mg-modified irons [54].

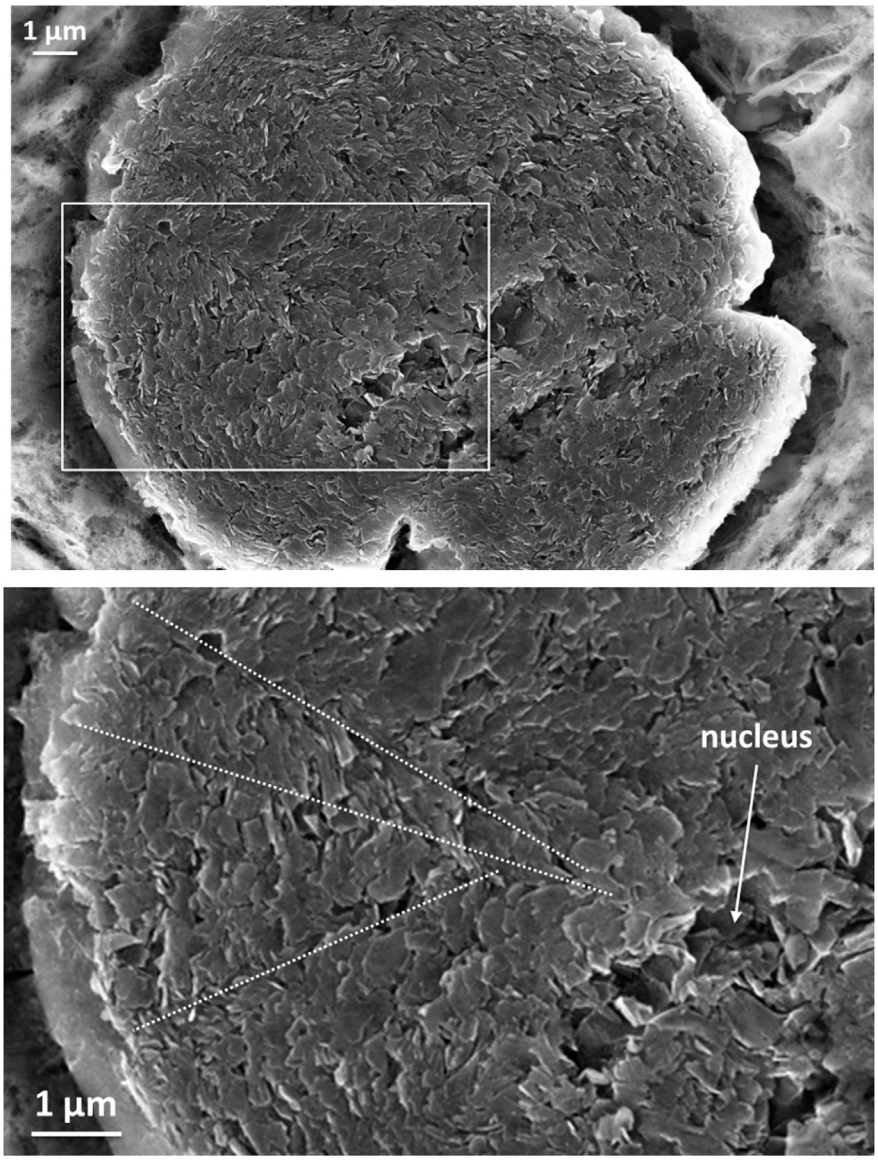

Fig. 24. Deep-etched SEM images of a graphite spheroid from series Q5CG at two magnifications: graphite platelets growing as foliated dendrites to form conical sectors.

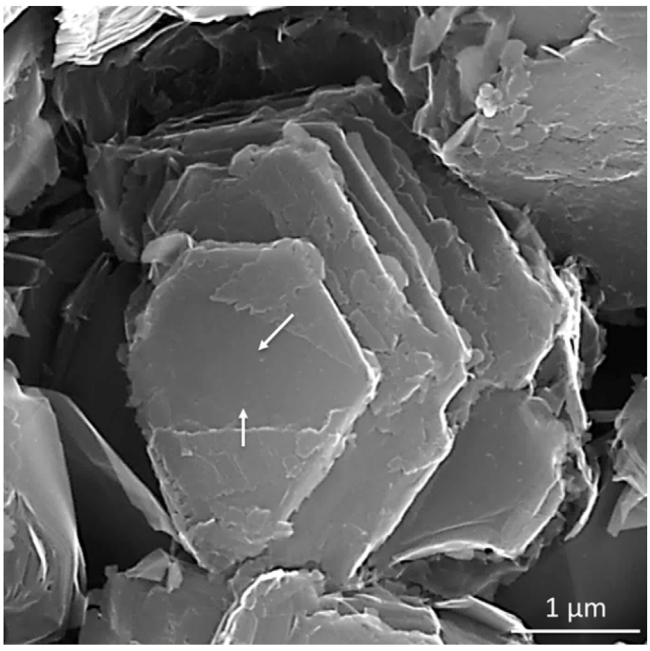

Fig. 25. Growth front of new graphene layers in a CG iron sample; the arrows indicate the direction of growth.

micrometers (Fig. 17). Growth of the aggregate is again in the *a*-direction of the platelets. While most platelets are oriented with the *a*-axis along the growth direction, many are not, showing the beginning of disorganization.

When small additions of 0.013% Mg were used, a mixed SG-CG-LG structure was found in the early stages of solidification (Fig. 13-b), while the room temperature graphite morphology was lamellar. The lamellar graphite warped extensively forming "curly" graphite as shown in Fig. 18 at two different fraction solid. What appears to be lamellae of curly graphite in 2-D, are clearly plates growing in the *a*-direction and curving around the *c*-axis, as seen in Fig. 18-b.

An increased Mg addition of 0.02% amplified compaction of graphite, producing a predominantly CG microstructure. Tadpole graphite appearing at $f_S > 0.45$ seems to be an assembly of Gr platelets stacked along their *c*-axis (Fig. 19-a). What appear to be a spheroid on 2-D, is a vertical growth of approximate cylindrical shape in 3-D. Initial CG aggregates are also the result of stacking of the graphite platelets, with significant *c*-direction dimension, close to that in the *a*-direction (Fig. 19-b). In addition, in compacted graphite the platelets are assembled into clusters of parallel platelets that have different orientations growing at an angle with respect to one another (Fig. 20). The clusters have a height of several microns, looking like graphite blocks under certain observation conditions.

Some graphite aggregates resembling what is commonly known as chunky graphite were also found in the 0.02% Mg samples. They grow radially from a common center and are the product of *c*-direction stacking of Gr platelets (Fig. 21).

SEM micrographs of deep etched room temperature CG iron samples exhibit the same pattern of growth identified for lamellar and tadpole graphite, i.e. stacking of graphite platelets (Fig. 22). However, the platelets spread both in the *a*- and *c*-direction over a wider area than for LG.

A variety of spheroids and imperfect spheroids were found in the early stages of solidification of Mg-treated irons. At the low Mg level of 0.013%, clear radial growth of dendritic appearance was observed (Fig. 23-a). Increase Mg level further moved graphite shape toward that of a spheroid, albeit imperfect ones. Graphite platelets were still observable on some of the spheroids (Fig. 23-b), with some of the platelets appearing to be perpendicular to the radius of the spheroid. The radial sectors become more compact,

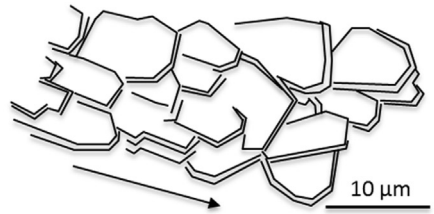

a) tiled-roof arrangement of platelets on a graphite lamella (no Mg)

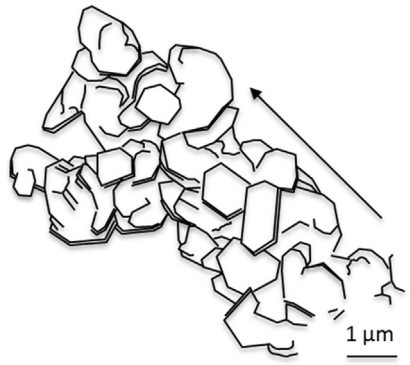

b) foliated dendrite of platelets on a graphite lamella (no Mg)

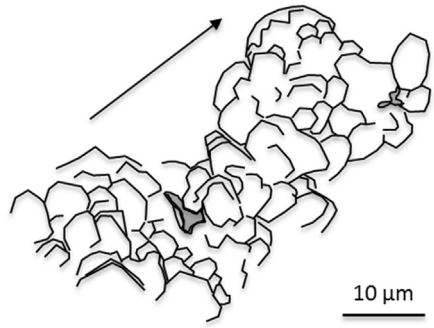

c) foliated dendrite of platelets on CG (0.013% Mg)

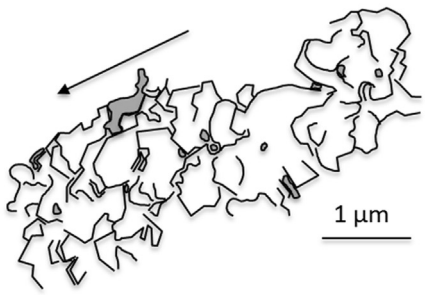

d) foliated dendrite of platelets on SG (0.02% Mg)

Fig. 26. Summary drawings of graphite aggregates based on SEM images; increased irregular shape of the (1010) surfaces as %Mg increases; gray regions are cavities resulting from the removal of the austenite by the deep etching; arrows are indicating the direction of growth.

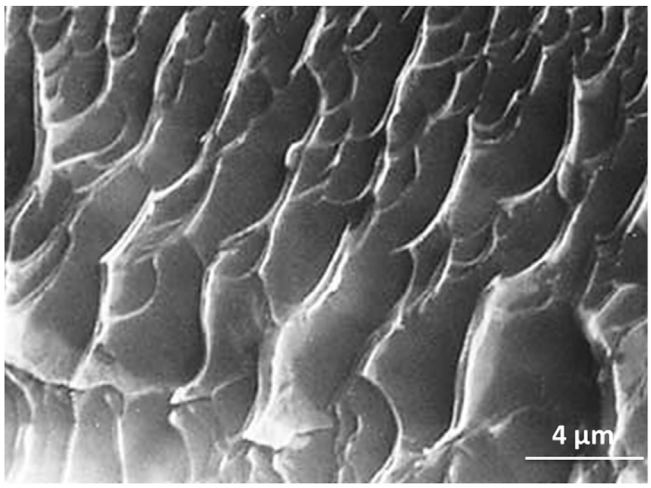

Fig. 27. SEM micrograph of a fractured graphite lamella showing tiled-roof configuration of graphite platelets [1].

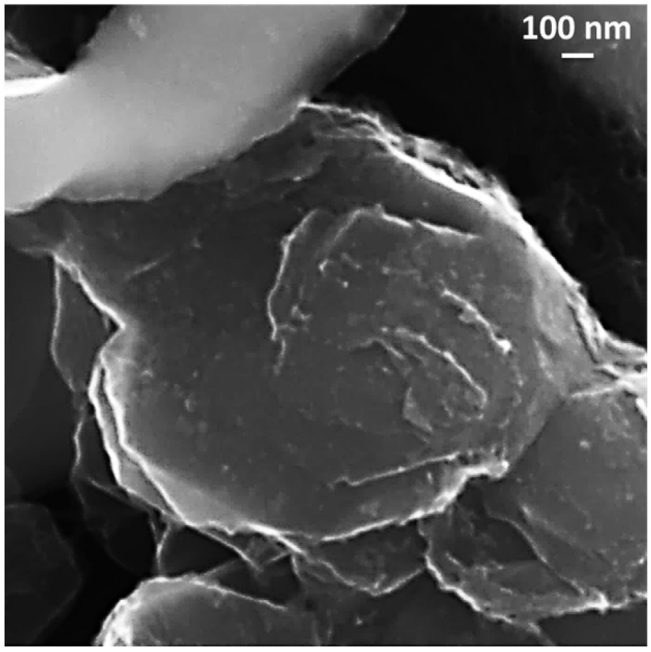

Fig. 28. Branching of a platelet on a graphite dendrite and *c*-axis rotational faults; new platelets grow at an angle with respect to the original one.

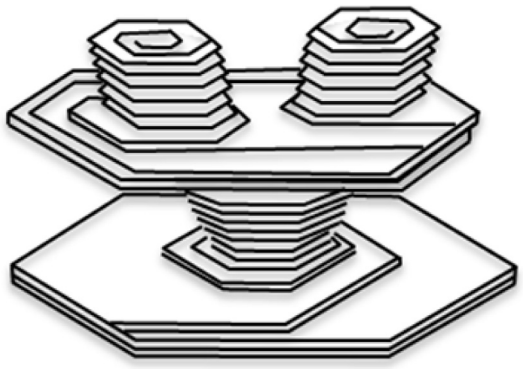

Fig. 29. Formation of protuberances and branching to produce a foliated crystal (after Saratovkin).

but still suggest growth from a common center (Fig. 23-c).

Higher magnification of another graphite spheroid (Fig. 24) reveals the platelet sub-structure. Growth is much disorganized around the nucleus that was removed by deep etching. While conical sectors of platelets growing radially away from the nucleus are seen, not all sectors originate in the nucleus. This is similar with what was found on ion-etched graphite nodules (Fig. 2-a). The large number of cavities between the platelets, which are regions where the austenite has been removed by the deep etching, is consistent with growth of foliated dendrites. There is no evidence of growth by rolling or wrapping of the graphene sheets.

4. Discussion

The results of the SEM investigation presented in the preceding paragraphs, as well as research of other investigators cited in this paper, demonstrate that LG, CG, chunky Gr, and SG all grow radially from a common center. The basic building blocks of the graphite aggregates are hexagonal faceted graphite platelets with nanometer height in the *c*-direction and micrometer width in the *a*-direction. Thickening of the platelets occurs through growth of additional graphene layers nucleated at the ledges of the graphite prism as shown in Fig. 25 for CG iron and in Fig. 16-b for LG iron.

In Mg-free LG irons, the platelets grow as layered crystals exhibiting a tiled-roof configuration (Fig. 26-a) or form foliated dendrites (Fig. 26-b). The tiled roof configuration was also observed through TEM (Fig. 27). Note the similitude between the drawing in Fig. 26-b, which is based on SEM micrographs, and the schematic drawing of foliated dendrites in Fig. 10-a. Branching of the foliated dendrites can occur at screw dislocation defects produced on the platelets (Fig. 28).

Foliated dendrites were also observed in Mg-modified CG irons (Figs. 22 and 26-c). However the graphite platelets stack along the *c*-axis building clusters of graphite platelets growing at various angles with respect to one another (Fig. 20). Quasi-cylindrical shapes connected to more or less curved walls (tadpole graphite) and compacted graphite were generated. Sometimes radial stacking of the platelets was observed. The hexagonal shape of the platelets is less regular, indicating a roughening of the interface produced by the higher constitutional undercooling induced by Mg.

As the Mg level further increases, chunky graphite and more spheroids crystallized from the melt. The chunky graphite aggregate is made of quasi-cylindrical sectors of graphite platelets stacked along the *c*-axis, growing radially from a common nucleus (Fig. 21). The graphite spheroids exhibit foliated dendrites growing radially from the center with many voids between the plates (Fig. 26-d). The platelets are more irregular than for the lower Mg iron. In general, as the amount of Mg increases, the platelets gradually lose their clear hexagonal shape observed in LG iron.

An attempt to integrate these observations in the existing body of knowledge will be presented. The current understanding is that various solutes in molten iron will affect the morphology of the growing graphite through a number of mechanisms including:

1. increased Gr/L interface undercooling because of the attachment of impurities (e.g. Mg, Ce, O) to the graphite surface, and rejection of solute (Mg, Bi, Pb, Sn) into the liquid;
2. decreased Gr/L interface undercooling because of lower surface energy ensuing the adsorption (weak van der Waals forces) of surface active elements (S,O);
3. change of the graphite crystal habitus because of the adsorption of reactive or surface active elements; this effect could also be understood in terms of bending of the graphene layer because of attachments of elements (see for example Fig. 11).

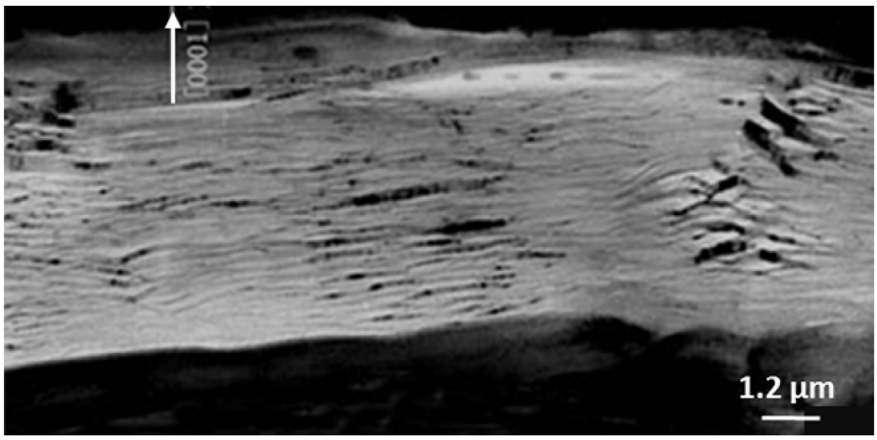

Fig. 30. TEM micrograph of a graphite lamella [1] exhibiting the pattern of a layered crystal with iron entrapped between the layers.

The solubility of Mg vapor in liquid iron at 1600 °C was measured to be 0.059% at 1 atm Mg pressure [55]. However, carbon and silicon significantly increase the solubility. In a 4%C iron alloy, the maximum solubility is 1.8% at 1427 °C. The addition of 3% Si to the above alloy raises the solubility to 2.3% Mg [56]. It is thus safe to assume that a Fe–C–Si melt may dissolve somewhere in the vicinity of 1% Mg at the solidification temperature. On the other hand, the solid solubility of Mg in iron is essentially zero at atmospheric pressure even at very high temperatures [57]. It follows that because of the very small partition coefficient, Mg-modified iron will exhibit increased constitutional undercooling as solidification advances. This will promote interface instability of the graphite platelets favoring developments of faceted dendrites.

From the SEM study presented in this work it is apparent that the growth of graphite crystals from Fe–C–Si melts can be described as foliated crystal and foliated dendrite growth. For faceted crystals such as graphite, because the kinetic limitation to growth of the facets is large, high constitutional undercooling is required to break down the plane interface [58]. The large amounts of impurities available in the melt (S, O, N, Mg, etc.) accumulate on the basal faces of the hexagonal graphite platelets and produce high constitutional undercooling. Screw dislocations generated at the leading edge of the graphite platelet may develop into protuberances (Fig. 29). The dislocation will continue to move in the *c*-direction, and the protuberance will increases in thickness. If the protuberance grows enough to reach a region with lower constitutional undercooling, the growth rate anisotropy of the crystal can re-assert itself, lateral growth occurs parallel to the first formed platelet, and a new platelet emerges. This pattern of growth results in layered (foliated) crystals. If two or more protuberances are produced on a platelet (a multiplication mechanism as the one suggested in Ref. [59] may be responsible), they will tend to grow divergently to optimize mass feeding to the growing surface, which results in branching.The process can be repeated to form a multilayered foliated dendrite.

The foliated dendrites will continue to expand in the *a*-direction, but also thicken through the classic mechanisms of two-dimensional nucleation and screw dislocation movement. Indeed, TEM micrographs of lamellar graphite show that a large number of iron containing regions are incorporate in the graphite (Fig. 30). A significant number of dark spots between the graphite platelets, deemed to be iron, were also identified in this work (e.g. Fig. 24).

Alternatively, the break-down of the hexagonal faces of the graphite because of the high constitutional undercooling may results in branching of the platelet as shown in Fig. 28.

Foliated dendrites of faceted phases, and transition to radial growth producing star-like dendrites with increased cooling rates, have been observed in other systems. The case of CdI_2 was discussed earlier. Another example is the dendritic growth of faceted Al_3Ti phase in an Al–Ti alloy [60] where "tiled-roof" structure and growth of protuberances to produce foliated dendrites were observed at low cooling rates. At higher cooling rates star-like shapes developed because two or more (001) plates grow perpendicular to each other from the same nucleus. Chernov [61] predicted that this shape can result from a progressively increasing solute content in the liquid from the tip towards the center of the plate edge, which must result in a progressively decreasing growth rate normal to the edge.

The dendritic structure of SG was advocated as early as1963 by Minkoff and Einbinder [62] who reported a dendritic form of graphite on an imperfect graphite spherulite found in a Ni–C melt. They further argued that every branch of the dendrite may be regarded as an independent columnar crystal grown from their own nucleus situated along the principal trunk of the dendrite. Hamasumi [4] identified graphite spheroids with protruding dendritic patterns, as shown in Fig. 31, in a large SG iron casting having 3.5% C and 2.85% Si. They could not confirm whether the dendritic pattern consists of a single crystal or many columnar crystals radiating from nuclei scattered along the principal axis of the dendrite.

To summarize, in all graphite forms investigated in this study, the overall growth direction of the aggregate is radial, and the appearance is dendritic. In melts with surface active elements (S, O, N), the graphite platelets grow initially parallel to one another when nucleated at the austenite/liquid interface, and then develop into layered crystals and foliated dendrites with the *a*-direction dimensions much larger than the *c*-direction ones. The *c*-direction of the platelets is perpendicular to the radius of the aggregate. This is lamellar graphite.

Upon Mg addition constitutional undercooling is increased. This destabilizes the (0001) faces of the graphite producing a rougher interface. Branching of the platelets followed by growth in various directions different from that of the initial platelet follows (Fig. 20). In addition to the twining faults, rotational stacking faults occur. Stacking of platelets in the *c*-direction becomes more significant and clusters with blocky appearance are produced. Although the effect of Mg on the graphene layers has not been documented, existing work with other elements such as oxygen [49], allows to

a) optical micrograph, x250

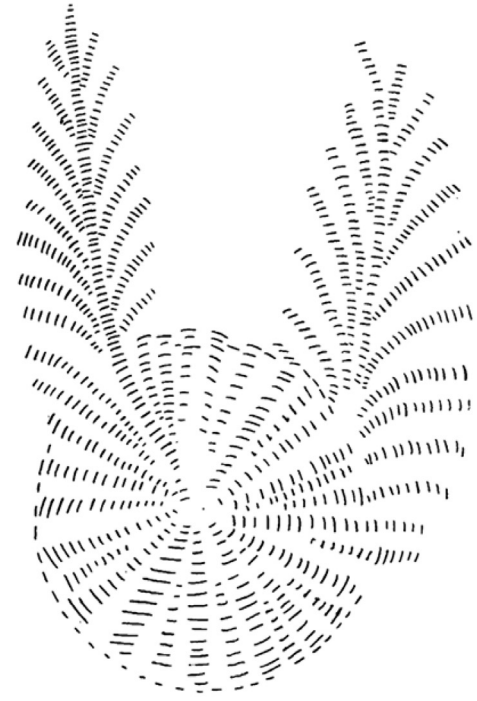

b) schematic representation

Fig. 31. Graphite spheroid with dendritic outgrowth [4].

postulate that curved platelets are formed because of the bending of the graphene layer induced by the attachments of Mg. Clusters of platelets with different orientation appear, although the overall aspect is still, in many cases, that of foliated dendrites. The overall graphite aggregate is thicker in the *c*-direction compared with the LG aggregate. This is compacted graphite. So far, the schematic representation in Fig. 7 seems to do a reasonable job in describing the growth of LG and CG.

At even higher Mg additions, while the overall growth of the graphite aggregate remains radial, the stacking of the platelets changes direction, occurring with the *c*-direction parallel to the radius of the aggregate. This produces chunky and spheroidal graphite. The growth of the platelets in the *c*-direction may occur through the foliated crystal mechanism. This does not require nucleation of the secondary branches of the dendrite, as the branching mechanisms of the graphite platelets identified in this paper can generate new dendrite arms. Limited helical growth (Double and Hellawell) may also be a growth mechanism involved in this process. There is SEM evidence for helical growth in the literature [31] and in this paper (Fig. 16-a), although not for complete conical helices. The result is a conical sector made of stacked graphite plates. Stacking of graphite plates was documented earlier for chunky graphite [31]. The conical sectors may occupy the whole volume of the sphere forming a graphite spheroid, or only part of it like in exploded graphite. Chunky graphite can be the product of a succession of conical sectors growing on top of one another.

Before concluding we need address one more issue. Many SEM pictures of SG iron exhibit a layer growth (cabbage type) on the surface of the graphite. Clearly the graphite grows in the *a*-direction, by a mechanism that seems to be analogous to that described by Sadocha and Gruzleski [14]. There is also TEM evidence of such growth for SG as shown in Fig. 32 [63] and HREM evidence for amorphous graphite growing in an electronic beam [64]. This growth pattern occurs after encapsulation of the graphite spheroid into an austenitic shell, when growth of the graphite continues through solid diffusion of carbon through the austenite to the growth front.

While this research has uncovered many of significant aspects of graphite crystallization from the liquid, unanswered questions still remain. In the opinion of these authors, understanding the exact role that Mg plays in changing the habitus of the graphite is of paramount importance, as it is significant to note that, at typical industrial cooling rates of 0.5–10 K/s, it is impossible to obtain well-rounded SG without Mg additions.

5. Conclusions

The results of the SEM investigation presented in this research indicate that most types of graphite crystallizing from Fe–C–Si melts grow radially from a common center as foliated crystals or dendrites, and are assemblies of hexagonal faceted graphite platelets with nanometer height in the *c*-direction and micrometer width in the *a*-direction. The platelets are thus considered to be the building blocks of graphite aggregates. The exception seems to be the graphite nucleating at the γ/L interface in low-S irons, where multiple nucleation of the graphite platelets was found, and the platelets grow parallel to one another before building foliated dendrites.

In Mg-free lamellar graphite irons, the platelets grow as foliated crystals with a tiled-roof configuration or as foliated dendrites. There was experimental evidence that thickening of the plates occurs through growth of additional graphene layers nucleated at the ledges of the graphite prism. Branching of the foliated dendrites was observed to occur at screw dislocation defects on the platelets. While foliated dendrites were also identified in Mg-modified irons;

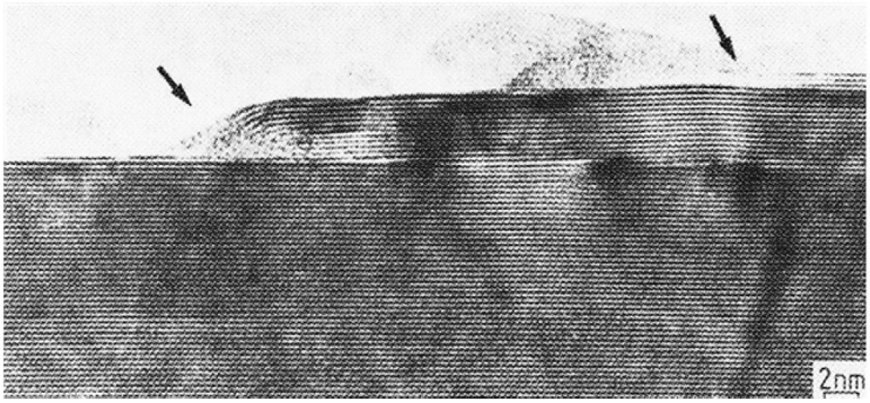

Fig. 32. TEM image of a fractured graphite spheroid showing crystallization sites (indicated by arrows) of amorphous graphite [63].

the graphite platelets stacked predominantly along the *c*-axis, producing clusters of blocky appearance. The clusters are oriented at various angles with respect to one another. This is typical for compacted graphite irons and tadpole graphite, in which the platelets spread in the *a*-direction and stack in the *c*-direction significantly more than for lamellar graphite iron, which explains the coarser appearance of CG as compared to LG on standard metallographic pictures.

The chunky graphite aggregates investigated are quasi-cylindrical sectors of platelets stacked along the *c*-axis, growing as foliated dendrites developing radially from a common nucleus. In the graphite spheroids examined in this work, the foliated dendrites form conical sectors adjacent to one another. The {1010} faces of the platelets composing these dendrites are less faceted than in the Mg-free irons.

References

[1] K.M. Fang, G.C. Wang, X. Wang, L. Huang, G.D. Deng, The microstructure and metamorphic regularity of graphite in cast iron, in: Y.X. Li, H.F. Shen, Q.G. Xu, Z.Q. Han (Eds.), Science and Processing of Cast Iron VIII, Tsinghua Univ. Press, Beijing, China, 2006, pp. 181–187.

[2] D.K. Bandyopadhyay, D.M. Stefanescu, I. Minkoff, S.K. Biswal, Structural transitions in directionally solidified spheroidal graphite cast iron, in: G. Ohira, T. Kusakawa, E. Niyama (Eds.), Physical Metallurgy of Cast Iron IV, Tokyo, Mat. Res. Soc. Proc., Pittsburgh, Pa., 1989, pp. 27–34.

[3] S. Amini, R. Abbaschian, Nucleation and growth kinetics of graphene layers from a molten phase, Carbon 51 (2013) 110–123.

[4] M. Hamasumi, A newly observed pattern of imperfect graphite spherulite in nodular iron, Trans. JIM 6 (1965) 234–239.

[5] D.M. Stefanescu, L. Dinescu, S. Craciun, M. Popescu, Production of vermicular graphite cast iron by operative control and correction of graphite shape, in: Proc. 46th Int. Foundry Congress, CIATF Madrid, Spain, 1979. Paper 37–1.

[6] A. Velichko, C. Holzapfel, F. Mücklich, 3D characterization of graphite morphologies in cast iron, Adv. Eng. Mater 9 (1–2) (2007) 39–45.

[7] B. Lux, Mem. Sci. Rev. Mett. LXVI (1969) 347.

[8] B. Lux, Giess. Forsch. 19 (1967) 141.

[9] M. Hatate, K. Nakamura, H. Sumimoto, Production of iron-base alloys with fine graphite and its physical properties, in: G. Ohira, T. Kusakawa, E. Niyama (Eds.), Physical Metallurgy of Cast Iron IV, Tokyo, Mat. Res. Soc. Proc., Pittsburgh, Pa, 1989, pp. 149–156.

[10] E. Aguado, D.M. Stefanescu, J. Sertucha, P. Larrañaga, R. Suárez, Effect of carbon equivalent and alloying elements on the tensile properties of superfine interdendritic graphite irons, Trans. AFS 122 (2014) 249–258.

[11] P.C. Liu, C.L. Li, D.H. Wu, C.R. Loper, SEM study of chunky graphite in heavy section ductile iron, Trans. AFS 91 (1983) 119–126.

[12] H. Itofuji, H. Uchikawa, Formation mechanism of chunky graphite in heavy-section ductile cast irons, Trans. AFS 98 (1990) 429–448.

[13] W. Oldfield, G.T. Geering, W.A. Tiller, Solidification of spheroidal and flake graphite cast iron, in: The Solidification of Metals, Iron and Steel Inst., London, Publication No. 110, 1967, p. 256.

[14] J.P. Sodocha, J.E. Gruzleski, The mechanism of graphite spheroid formation in pure Fe-C-Si alloys, in: B. Lux, I. Minkoff, F. Mollard (Eds.), The Metallurgy of Cast Iron, Georgi Publishing Co., St. Saphorin, Switzerland, 1974, pp. pp.443–459.

[15] B. Dhindaw, J.D. Verhoeven, Nodular graphite formation in vacuum melted high purity Fe-C-Si alloys, Metall. Trans. A 11A (1980) 1049–1057.

[16] D.D. Double, A. Hellawell, The nucleation and growth of graphite-the modification of cast iron, Acta Metall. Mater 43 (1995) 2435–2442.

[17] R.W.G. Wyckoff, Crystal Structures, Interscience, New York 1, 1963.

[18] M.S. Dresselhaus, G. Dresselhaus, K. Surihara, I.L. Spain, H.A. Goldberg, Graphite Fibers and Filaments, in: Springer Series in Materials Science, 5, 1988.

[19] E.V. Zakhartchenko, E.P. Akimov, C.R. Loper, Kish graphite in gray cast iron, Trans. AFS 87 (1979) 471–476.

[20] A.N. Roviglione, J.D. Hermida, From flake to nodular: a new theory of morphological modification in gray cast iron, Metall. Mater. Trans. 35B (2004) 313–330.

[21] D.D. Double, A. Hellawell, The structure of flake graphite in Ni-C eutectic alloy, Acta Metall. 17 (1969) 1071–1083.

[22] W. Bollman, B. Lux, Grain boundaries in graphite, in: B. Lux, I. Minkoff, F. Mollard (Eds.), The Metallurgy of Cast Iron, Georgi Publishing Co., St Saphorin, Switzerland, 1975, pp. 461–470.

[23] D.D. Double, A. Hellawell, Growth structure of various forms of graphite, in: B. Lux, I. Minkoff, F. Mollard (Eds.), The Metallurgy of Cast Iron, Georgi Publishing Co., St Saphorin, Switzerland, 1975, pp. 509–528.

[24] C. Cosneanu, Metal. Rom. 10 (1966) 563.

[25] J. Keverian, H.F. Taylor, J. Wulff, Am. Foundrym. 23 (1953) 85.

[26] K.I. Washchenko, A.P. Rudoy, Surface tension of cast iron, Trans. AFS 70 (1962) 855.

[27] R.H. McSwain, C.E. Bates, Surface and interfacial energy relationships controlling graphite formation in cast iron, in: B. Lux, I. Minkoff, F. Mollard (Eds.), The Metallurgy of Cast Iron, Georgi Publishing Co., St Saphorin, Switzerland, 1975, pp. 423–442.

[28] W.C. Johnson, H.B. Smartt, The role of interphase boundary adsorption in the formation of spheroidal graphite in cast iron, Metall. Trans. A 8A (1977) 553–565.

[29] J.S. Park, J.D. Verhoeven, Transitions between type A flake, type D flake, and coral graphite eutectic structures in cast irons, Metall. Mater. Trans. A 27A (1996) 2740–2753.

[30] T. Skaland, Nucleation mechanisms in ductile iron, in: Proc. AFS Cast Iron Inoculation Conf., AFS, Schaumburg, Il, 2005, pp. 13–30.

[31] D.M. Stefanescu, Science and Engineering of Casting Solidification, third ed., Springer, 2015.

[32] D.M. Stefanescu, F. Martinez, I.G. Chen, Solidification behavior of hypoeutectic and eutectic compacted graphite cast irons, chilling tendency and eutectic cells, Trans. AFS 91 (1983) 205–216.

[33] X.J. Deng, P.Y. Zhu, Q.F. Liu, Structure and formation of vermicular graphite, AFS Trans. 94 (1986) 927–934.

[34] S.I. Karsay, E. Compomanes, Control of graphite structure in heavy ductile iron casting, AFS Trans. 92 (1970) 85–92.

[35] I. Minkoff, The Physical Metallurgy of Cast Iron, John Wiley & Sons, 1983.

[36] R. Elliott, Eutectic Solidification Processing, Butterworth, London, 1983.

[37] D.M. Stefanescu, Cast iron, in: D.M. Stefanescu (Ed.), ASM Handbook, Casting, 15, ASM International, Metals Park, Ohio, 1988, pp. 168–181.

[38] K. Herfurth, Freiberg Forschungs 105 (1965) 267.

[39] A. De Sy, Met. Progr 55 (1949) 138.

[40] F.H. Buttner, H.F. Taylor, J. Wulff, Am. Foundrym. 20 (4) (1951) 49.

[41] B. Marincek, et al., Giess. Techn. Wiss. Beih 12 (1953) 587.

[42] B.S. Milman, Litejnoe Proizv. 6 (1958) 11–17.

[43] H. Geilenberg, Giess. Techn. Wiss. Beih 16 (1964) 35.

[44] F.C. Frank, in Doremus, Roberts, Turnbull (Eds.), Growth and Perfection of Crystals, John Wiley NY, 1958.

[45] K. Theuwissen, J. Lacaze, L. Laffont, Structure of graphite precipitates in cast iron, Carbon (2015), http://dx.doi.org/10.1016/j.carbon.2015.10.066.

[46] D.D. Saratovkin, Dendritic Crystallization, Consultants Bureau, New York, NY, 1959.

[47] S.H. Yoon, S. Lim, S.H. Hong, W. Qiao, D.D. Whitehurst, I. Mochida, et al., A conceptual model for the structure of catalytically grown carbon nano-

fibers, Carbon 43 (2005) 1828–1838.
[48] G. Alonso, D.M. Stefanescu, P. Larrañaga, R. Suarez, Understanding compacted graphite iron solidification through interrupted solidification experiments, Int. J. Cast Metals Res. (2015), http://dx.doi.org/10.1179/1743133615Y.0000000020. Published on line.
[49] H.M. Muhmond, H. Fredriksson, Relationship between the trace elements and graphite growth morphologies in cast iron, Metall. Mater. Trans. 45A (2014) 6187–6199.
[50] G. Alonso, D.M. Stefanescu, P. Larrañaga, J. Sertucha, R. Suárez, Gray cast iron with high austenite-to-eutectic ratio Part I – calculation and experimental evaluation of the fraction of primary austenite in cast iron, Trans. AFS 120 (2012) 329–335.
[51] D.M. Stefanescu, G. Alonso, P. Larrañaga, R. Suarez, On the stable eutectic solidification of Iron-Carbon-Silicon alloys, Acta mater 103 (2016) 103–114.
[52] G. Alonso, D.M. Stefanescu, P. Larrañaga, R. Suarez, Understanding compacted graphite iron solidification through interrupted solidification experiments, in: R. Boeri, J. Massone, G. Rivera (Eds.), Proc. 10th Science and Processing of Cast Iron – CD, Mar del Plata, Argentina, 2014. Paper 1.
[53] E. Moumeni, N.S. Tiedje, A. Horsewell, J.H Hattel, A TEM study on the microstructure of fine flaky graphite, in: 52nd International Foundry Conference, Portoroz, Slovenia, 2012.
[54] G. Alonso, D.M. Stefanescu, P. Larranaga, R. Suarez, Understanding compacted graphite iron solidification through interrupted solidification experiments, Int. J. Cast. Met. Res. (2015), http://dx.doi.org/10.1179/1743133615Y.0000000020. Published on line.
[55] X. Zhang, Q. Han, D. Chen, Dissolution equilibrium of magnesium vapor in liquid iron, Metall. Trans. B 22B (1991) 918–921.
[56] P. Trojan, R. Flinn, Fundamentals of magnesium addition to ductile iron, SAE Tech. Pap. 640802 (1964), http://dx.doi.org/10.4271/640802.
[57] F.N. Tavadze, E.S. Kartoziya, A.Y.A. Shinyaev, Solubility of magnesium in iron, Metal Sci. Heat Treat. 3 (1) (1961) 25–26.
[58] M.C. Flemings, Solidification Processing, in: McGraw Hill Series in Mat. Sci. Eng., McGraw Hill, New York, 1974.
[59] Y. Liu, S. Yang, Growth mode and modification of graphite in cast iron melt, Acta Metall. Sin. B 5 (4) (1992) 263–267.
[60] D.H. St John, L.M. Hogan, Metallography and growth crystallography of Al_3Ti in Al-Ti alloys up to 5 wt% Ti, J. Cryst. Growth 46 (1979) 387–398.
[61] A.A. Chernov, Stability of faceted shapes, J. Cryst. Growth 24/25 (1974) 11–31.
[62] I. Minkoff, I. Einbinder, Official exchange paper – Israel, in: International Foundry Congress, 1963, pp. 139–143.
[63] G.R. Purdy, M. Audier, Electron microscopical observations of graphite in cast irons, in: H. Fredriksson, M. Hillert (Eds.), The Physical Metallurgy of Cast Iron, Stockholm, Mat. Res. Soc. Symposia Proc., North-Holland, NY, 1985, pp. 13–23.
[64] D. Ugarte, Curling and closure of graphitic networks under electron-beam irradiation, Nat. Lond. 359 (1992) 707–709.